https://doi.org/10.5194/egusphere-2026-5531
Preprint. Discussion started: 18 September 2026




# Characteristics of desert dust optical and physical properties from AERONET: spectral absorption, size distributions and spectral AOD

Thomas F. Eck[1,2], Jeffrey S. Reid[3], Alexander Sinyuk[4,2], Pawan Gupta[2], Antti Arola[5], Ilya Slutsker[4,2], Brent N. Holben[2], Philippe Goloub[6], Oleg Dubovik[6], Joel S. Schafer[4,2], Mikhail G. Sorokin[4,2], Alexander Smirnov[4,2], Hongbin Yu[2], Dongchul Kim[1,2], Elena Lind[2], Jason Kraft[7,2], Elizabeth A. Reid[3], Aboubacry Diallo[8], Thierno Ndiaye[8], Africa Barreto[9], Sidi Baika[10], Lahouari Zeudmi-Sahraoui[10], Francisco Evora[11], Gael Dubois[6], Luc Blarel[6], Rachel T. Pinker[12], Isaac Abiodun Adimula[13], Jean Louis Rajot[14], Aliko Maman[15], Muguette Allegre[14], Cassandra Gaston[16], Peter Sealy[16], Edmund Blades[16], Rebecca Chewitt-Lucas[17], Ian Lau[18], David Barker[19], Adel Saad Alshihiween[20], Abdulrahman Alsaferan[20], Odbayar Mishigdorj[21], Chogsom Jargalsaixan[22]

[1]University of Maryland Baltimore County, Baltimore, MD, USA
[2]NASA/GSFC, Greenbelt, MD, USA
[3]US Naval Research Laboratory, Monterey, CA, USA
[4]Science Systems Applications, Inc., Lanham, MD, USA
[5]Finnish Meteorological Institute, Kuopio, Finland
[6]Université des Sciences et Technologies de Lille, Laboratoire d'Optique Atmosphérique (LOA), France
[7]Fibertek Inc., Herndon, VA, USA
[8]IRD Institut de Recherche pour le Developpement Dakar Belair, Senegal
[9]Izana Atmospheric Research Center, Meteorological State Agency of Spain, Spain
[10]Office National de la Météorologie, Département Météorologique Régional Sud, Tamanrasset, Algeria
[11]Instituto Nacional de Meteorologia e Geofisica, Ilha do Sal, Cape Verde
[12]Department of Meteorology, University of Maryland, College Park, MD, USA
[13]University of Ilorin, Ilorin, Nigeria
[14]Laboratoire Interuniversitaire des Systemes Atmospheriques, Universite Paris Est – Creteil, France
[15]IRD - Institut de Recherche pour le Developpement, Niamey, Niger
[16]Rosenstiel School of Marine, Atmospheric, and Earth Science, University of Miami, Miami, FL, USA
[17]Caribbean Institute for Meteorology and Hydrology, Husbands, St. James, Barbados
[18]CSIRO Mineral Resources, Kensington, Western Australia, Australia
[19]CSIRO Environment, Aspendale, Victoria, Australia
[20]Energy Research Institute, King Abdulaziz City for Science and Technology, Riyadh, Saudi Arabia
[21]Information and Research Institute of Meteorology, Hydrology and Environment, Ulaanbaatar, Mongolia
[22]Meteorology Office, Dalanzadgad, Mongolia

*Correspondence to*: Thomas F. Eck (Thomas.F.Eck@nasa.gov)

https://doi.org/10.5194/egusphere-2026-5531
Preprint. Discussion started: 18 September 2026




**Abstract**

The AERONET multi-decade global database is examined to investigate long-term averages of retrieved physical and optical properties and spectral aerosol optical depth (AOD) of significant events at sites in major global dust source and receptor regions. After examples are shown of retrieved particle size and properties such as absorption, attention is paid to average spectral single scattering albedo (SSA) with comparisons to the laboratory measurements of dust from soil samples by Di Biagio et al. (2019). Overall, the AERONET retrieved and laboratory SSA agree very well for specific dust source regions in the Sahara and Sahel, with some regions showing annual cycles at 440 nm, an indicator of changes in iron oxide content. The strongest dust absorption was measured at an Australia desert site, and the least absorption was in dust transported to the Caribbean from the Sahara/Sahel regions. Also notable is regional and seasonal variability in the prevalence of ~0.3 to 1 μm radius dust, especially in the Sahel and Sahara. Such middle mode dust can often account for ~40% of AOD at 440 nm. These 'middle mode' sized particles are a probable significant contributor for the observed relatively large spectral drop-off in AOD in the wavelengths beyond the visible, at 1020 nm and especially 1640 nm, in most dust events where Angstrom Exponent is low. Increased understanding of absorption, size distributions and AOD spectra of dust aerosol may help in improving remote sensing retrievals plus in more accurately characterizing the radiative effects of desert dust.

## 1. Introduction

Environmental impacts of airborne desert dust particles are varied and extensive including perturbation of both solar and terrestrial radiation budget of the Earth-atmosphere system (Carlson and Benjamin, 1980; Otto et al., 2007; Kok et al., 2017; Obiso et al, 2024), adverse effects on human health (Yang et al., 2022), fertilization of ocean waters (Bishop et al., 2002; Westberry et al., 2023) and the Amazon rainforest (Swap et al., 1992; Rizzolo et al., 2017; Yu et al., 2015), reductions in efficiency of solar energy installations (Li et al., 2020; Sayyah et al., 2014) and potential influences or covariances with hurricane formation/intensity (Sun et al., 2008; Rosenfeld et al., 2012; Xian et al., 2020). At the same time dust is well known to have strong seasonal/interseason variability and trends by continent and region, (e.g., Formenti et al. 2011; Alfaro-Conreras et al., 2017; Mitchell et al. 2017; Gavrouzou et al. 2021; Zhang et al. 2025). Indeed, the interplay between meteorology, orography, and soil erosion susceptibility is complex as is its upscaling. For example, Evan et al. (2016) analyzed long-term climatic variability in meteorology and dust emission from the Sahara and Sahel, suggesting that surface wind in conjunction with surface topography (which locally increases wind speed) is a primary factor in dust emissions at this time scale. They found that within the last ~50 years dust emission in this region was high in the 1970s and 1980s and especially low in the 2000's, the latter of which is the time interval of the AERONET data sets we present in this current work. Climate modeling by Evan et al. (2016) suggest that future climate change associated with greenhouse gas increases may slow the tropical circulation and therefore reduce future dust emission in this largest global dust source region.

Complexity in dust's emission patterns are mirrored in their chemical, microphysical and consequently optical properties. Indeed, while at the grossest levels, we think of airborne dust as a monolithic specie (e.g., coarse mode dominated, strong absorbing in the blue to ultraviolet (UV) wavelength regions, and AOD as spectrally flat) in fact higher order applications related to radiative transfer and geochemical cycles are fraught with subtleties and nuance.

https://doi.org/10.5194/egusphere-2026-5531
Preprint. Discussion started: 18 September 2026




For example, ocean fertilization by dust is dependent on iron oxidation state. This same oxidation state relates to shortwave absorption and ultimately its net impact on atmospheric forcing (e.g., Li et al. 2021; Obiso et al. 2024). Intertwined is variability in dust chemistry and particle size (e.g., Reid et al., 2003a; Reid et al., 2008 to more recently Panta et al. 2023). Size/chemistry relationships then project onto a) the thermal infrared, in particular for giant mode particles (Gonçalves Ageitos et al. 2023; Li et al. 2025) to b) health effects where fine mode dust has higher penetration and leads to numerous health disorders (Goudie, 2014; Lwin et al., 2023; Proestakis et al, 2025). And finally, all of the above have dependencies back to meteorology and large-scale transport (Maringet al., 2003; Reid et al., 2008 to more recently Formenti and DiBiagio, 2024; Kim et al. 2024; Proestakis et al, 2024).

Noteworthy in all manner of global dust research is the federated Aerosol Robotic Network (AERONET; Holben et al. 1998) providing systematic measurement of Aerosol Optical Depth (AOD) and sun sky retrievals of size, refractive index, spectral absorption, asymmetry parameter/phase function (Dubovik and King, 2000; Dubovik et al., 2006). From this numerous global climatologies have been developed (e.g., starting with Holben et al., 2001; Dubovik et al., 2002). This current work is in certain aspects an update and further expansion on the paper of Kim et al. (2011) that provided a study of the dust measurements and retrievals from AERONET instruments located in the Sahel, Sahara and Arabian Peninsula utilizing the Version 2 database which was much less extensive than the current V3 database. Ultimately, AERONETs global distribution of sites, and well characterized globally consistent data products has led to thousands of citations for its use. As an example just in the past few years, researchers have leveraged AERONET data, including Single Scattering Albedo (SSA), particle size, and spectral AOD for the validation and comparison of airborne dust optical properties derived from satellite observations and model simulations on topics listed above (e.g., Li, D. et al., 2025; Gonçalves Ageitos et al., 2023; Lyapustin et al., 2021; Go et al., 2025; Li et al., 2024; Li, L. et al., 2025; Obiso et al., 2024; Proestakis et al., 2024; Song et al., 2021; Wang et al., 2024; Yu et al., 2021; Yus-Díez et al., 2025; Zhao et al., 2023; Zheng et al., 2023).

While it is gratifying that AERONET sees such widespread utility, the many studies that employ its data products often do so under fairly narrow scope (e.g., limited time periods and areas for specific topics such as satellite verification). The dataset is now large enough to revisit key aspects of retrieved dust properties, and their relative modalities in regard to location and seasonality. This paper represents an effort to systematically examine retrieved dust properties for the major global emission regions and downwind, in order to evaluate and enhance understanding of this widely utilized database.

## 2. Instrumentation, Data and Methodology

### 2.1 AERONET instruments and measurement of AOD

AERONET's surface-based remote sensing network utilizes the Cimel Electronique CE-318 sun-sky radiometer for measurements of AOD and directional sun-sky radiances in its global network (see Holben et al., 1998) The CE-318 automatically tracks the sun to provide AOD and sky radiance for retrievals with a ~1.25° full field of view. There are some instrument variations between dates and sites, but in this study the standard instrument configuration for many instruments was used with AOD measurements at seven or eight wavelengths (340, 380, 440, 500, 675, 870, 1020, plus 1640 nm for newer models), and 940 nm for water vapor retrieval. Some earlier instruments in the Sahel region (some pre-2012; others till pre-2021) only measured AOD at four wavelengths: 440, 675, 870 and 1020

https://doi.org/10.5194/egusphere-2026-5531
Preprint. Discussion started: 18 September 2026




nm so that polarization measurements could be made. Sampling rates also varied by site and date, with some sites attempting an AOD measurement every 15 minutes, while most over the last 5-8 years made measurements approximately every 5 min to obtain high temporal resolution data.

It takes ~8 seconds to scan all wavelengths utilizing a motor driven filter wheel to position each filter in front of the detector, with three repeated measurement sets within a minute, to provide an ensemble mean and variance information for cloud screening. Ion assisted deposition interference filters were used with full width at half maximum bandpass of 2 nm at 340 nm, 4 nm for 380 nm, 10 nm for 440, 500, 675, and 1020 nm, and 25 nm at 1640 nm. The estimated uncertainty in AERONET measured AOD, due primarily to calibration uncertainty, is ~0.01-0.02 at optical airmass of one (directly overhead sun) for network field instruments (with the largest errors in the UV; Eck et al., 1999). This estimate is consistent with Schmid et al. (1999) who compared AOD values derived from 4 different solar radiometers (including an AERONET sun-sky radiometer) operating simultaneously together in field conditions and found that the AOD values from 380 to 1020 nm agreed to within 0.015 (root mean squared). More recently, Barreto et al. (2016) found similar results with the latest version of the Cimel sun-sky radiometer. The AOD uncertainty of AERONET reference calibration instruments is significantly better at ~0.002 to ~0.009, again with the higher errors in the UV (Eck et al., 1999) since these instruments are calibrated by the Langley technique at the stable high latitude Mauna Loa Observatory, Hawaii or Izaña Observatory, Spain (Shaw et al., 1983; Toledano et al. 2018). The uncertainty in the UV is higher due to slightly poorer repeatability of the Langleys Vo's and also due to inexact filter function transmittance characterization and possible temperature effects. The sky radiances are calibrated versus frequently characterized integrating spheres at the NASA Goddard Space Flight Center, assumed to have an absolute accuracy of ~3% (Sinyuk et al., 2020) in Version 3.

Except where noted, all AOD presented here are from direct sun measurements of level 2 AOD data (post calibrated and cloud screened) in the current Version 3 spectral AOD product described in detail by Giles et al. (2019). The complete set of Version 3 cloud screening and quality assurance algorithms are presented and analyzed in Giles et al. (2019).

The Angstrom Exponent (AE) is used as a gross indicator of particle size, in this study using low values as an indicator of a large particle/coarse mode dominated dust aerosol environment. AE values presented in this paper are operationally generated by AERONET and computed from linear regression in logarithmic coordinates of the measured AOD at four wavelengths (440, 500, 675 and 870 nm).

**Figure 1** provides an overview of the nine principal AERONET sites used in this assessment. Sites are numbered and overlaid on the MERRA-2 mean dust Optical Depth (AOD) from 2015 through 2025 (Randles et al., 2017). Sites were selected based on their longevity and location as receptors for major dust source regions. Dakar, Cabo Verde, and Ragged Point represent the large dust plumes exiting the Sahara and transporting across the Tropical Atlantic. Tamanrasset is recognized as a central Sahara receptor site (Guirado et al., 2014), notable for observations of a broad-spectrum absorbing dust, goethite, compared to the more common blue-dominated absorbing hematite (Go et al., 2022). Banizoumbou and Ilorin are receptors for the Bodélé Depression, widely considered one of the most significant single dust sources in the world (Washington et al., 2009). The longest-running receptor site in Southwest Asia was Solar Village in Saudi Arabia; similarly, Dalanzadgad, Mongolia, serves as a receptor for the

https://doi.org/10.5194/egusphere-2026-5531
Preprint. Discussion started: 18 September 2026




Taklimakan and Gobi deserts. Despite the arid nature of the Outback, Australia exhibits a relatively low dust prevalence compared to the other regions studied here. However, the Birdsville site is strategically located adjacent to the Simpson desert for regional characterization.

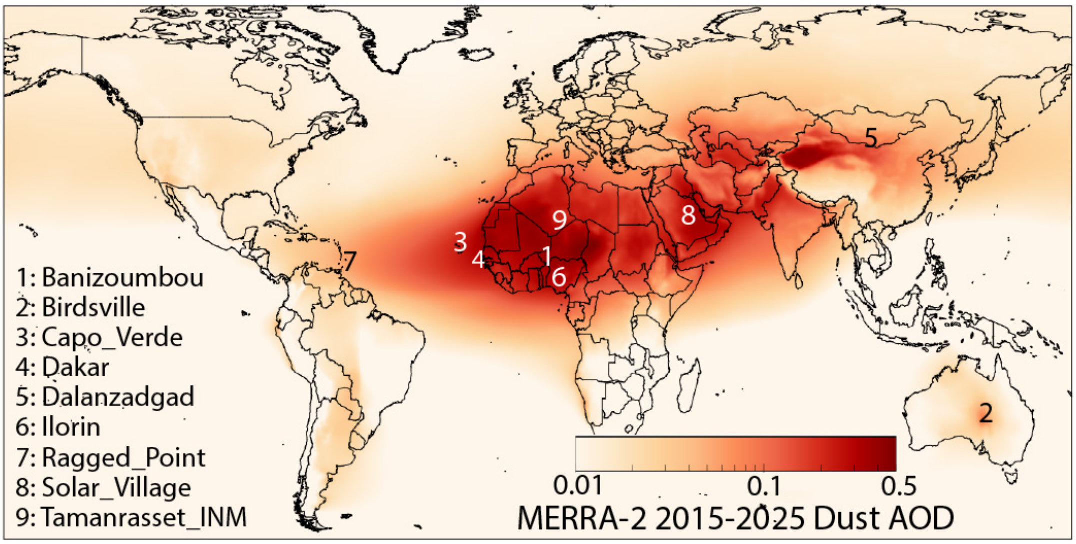


**Figure 1. The nine principal AERONET sites analyzed in this study located on a MERRA-2 derived global map of dust AOD, plotted on a logarithmic scale and averaged over the interval 2015-2025.**

### 2.2 AERONET Inversion Methodology

The almucantar sky radiance scans made by the newer Model-T version Cimel instruments are performed at fixed elevation angles equal to the solar elevation with ±180° azimuthal sweeps made sequentially at seven wavelengths (380, 440, 500, 675, 870, 1020 and 1640 nm). However in the standard V3 retrieval product only the data from 440, 675, 870 and 1020 nm (wavelengths measured by all models of Cimel instruments) are input to the inversion algorithm. These are made in both the morning and afternoon hours at optical airmasses of 4, 3, 2, and 1.7 (75, 70, 60, 54 degrees solar zenith angle, or SZA, respectively) plus once per hour in between. AERONET retrievals are also made utilizing hybrid sky scans with the new Cimel instruments version Model-T. The sky scan made with the hybrid methodology involves the instrument moving simultaneously in both the azimuthal and zenith angle directions, thus performing a scan that is in general intermediate between the almucantar and principal plane (principal plane scan varies the zenith angle while maintaining a fixed azimuth across the sun).

Hybrid and almucantar directional scan radiance data are individually combined with measured AOD data at identical wavelengths as inputs to retrieve optically equivalent column-integrated volume size distributions and aerosol refractive indices utilizing the algorithms as developed by Dubovik and King (2000) and Dubovik et al. (2006). These retrieved aerosol properties are utilized to derive additional parameters such as single scattering albedo, asymmetry parameter and phase function. The Version 3 Level 2 retrievals with the quality controls described in Holben et al. (2006) are presented in this study (see Sinyuk et al., 2020 for details). The percentage

https://doi.org/10.5194/egusphere-2026-5531
Preprint. Discussion started: 18 September 2026




particles of spheroidal and spherical shape required to give the best fit to the measured angular distribution of spectral sky radiances is also determined by the AERONET retrieval algorithm. Dubovik et al. (2006) provides further details on these retrieval algorithms.

In order to ensure sky radiance measurements over a sufficiently wide range of scattering angles in this study, only almucantar scans taken at solar zenith angles greater than ~50 degrees (optical airmass ~1.56) are analyzed and presented. The scattering angle range of measured sky radiances for an almucantar scan performed at 50 degrees SZA is 100 degrees while at 75 degrees SZA it is 150 degrees. However, the newly developed hybrid scans available only with the recent Model-T Cimels can provide directional sky radiance measurements with 100 degrees scattering angle range at a solar zenith angle of only 25 degrees. Additional cloud screening for hybrid and almucantar sky radiance measurements (first the AOD must pass the level 2 quality control and cloud screening) was performed through the requirement of symmetrical sky radiances on both sides of the sun at equal scattering angles. These radiances from both sides of the scan that meet the symmetry threshold are then averaged before being used as input to the AERONET retrieval. Directional sky radiance measurements that are asymmetrical at a given scattering angle (due to inhomogeneous aerosol distributions or cloud on one side) are eliminated, and a retrieval only reaches Level 2 when the required minimum number of measurements in defined scattering angle ranges are met (see Holben et al., 2006). Dubovik et al. (2000) found these AERONET inversions to be stable as determined by perturbation analyses accounting for random errors, instrumental data offsets and known uncertainties in the atmospheric radiation model. Sinyuk et al. (2020) found excellent agreement between almucantar and hybrid scan retrievals made within 12 minutes of each other.

In this study, we followed the guidance from Dubovik et al. (2000) and the V3 database for Level 2 quality control (Sinyuk et al., 2020) that only almucantar retrievals where 440 nm AOD is greater than 0.4 be used for analysis of spectral refractive indices and single scattering albedo. This paper utilizes the Version 3 AERONET database and data products. All of the V3 retrievals presented for multi-year analyses are level 2 data. However, we do present one individual retrieval case of a Level 1.5 almucantar retrieval when the minimum solar zenith angle threshold of 50 degrees was not met, having a SZA=43 degrees however the very high AOD in this case (~3.2 at 440 nm) substantially increased the retrieval sensitivity and accuracy.

**2.3 Retrieval product verification**

Unlike AOD, for sun sky retrievals products there is no method of absolute calibration and this can be as much of a challenge for the in situ observations as it is for the retrieval. However, numerous studies have compared retrieved products and in situ observations to show skill and physical consistency. Starting with fine mode dominated at the regional level, for biomass burning particles Reid et al. (2005) compared regional mean volume median radii from source regions in southern Africa, South America, boreal zone and temperate North America and found that AERONET retrievals versus *in situ* measurements of the diameter of fine mode particles were often within ~0.01 µm of each other. Over the Arabian Sea for fine mode pollution particles observed during the INDOEX experiment, Clarke et al. (2002) showed volume size distribution lognormal fits from both aircraft and ship in situ measurements

https://doi.org/10.5194/egusphere-2026-5531
Preprint. Discussion started: 18 September 2026




where the average accumulation mode volume peak radius values under high aerosol loading conditions ranged from 0.17 µm to 0.18 µm with corresponding geometric standard deviations (widths) of 1.51 (for ship) and 1.43 (for aircraft). This compares very well to AERONET retrievals made at Kaashidhoo Island in the Maldives (in the INDOEX region), for observations when $AOD_{440}$>0.4, of median radius of 0.18 µm and width of 1.49 (1998-2000 multi-year average Version 2 values). More recently, Schafer et al. (2019) compared time and location matched in situ measured fine mode size distributions from aircraft profiles with AERONET retrievals at three locations in the US. They found that when the in situ data were corrected for ambient RH conditions the agreement with the remote sensing retrievals was excellent, with fine mode peak radius differences averaging ~0.01 µm.

For larger sub-micron size Pinatubo eruption aged volcanic-stratospheric aerosols, Eck et al. (2010) discussed the relatively close agreement between *in situ* observations from stratospheric aircraft of 0.53 µm effective radius as reported by Pueschel et al. (1994) to AERONET retrievals made from observations in 1993 of ~0.56 µm peak volume radius.

For coarse mode dominated environments with super-micron radius particles, Reid et al. (2003b, 2006, 2008) found excellent agreement between AERONET retrieved and *in situ* measured size for both sea salt and desert dust aerosol. For aerosols of maritime origin, Smirnov et al. (2003) showed reasonable agreement between AERONET retrievals and in situ measurements of sea salt dominated coarse mode size distributions. Additionally, for coarse mode dust size distributions in the Sahel region of West Africa, Johnson and Osborne (2011) have shown good agreement between AERONET retrievals and in situ measurements from aircraft.

Regarding absorption, in southern Africa, for strongly absorbing fine mode dominated biomass burning aerosols, Leahy et al. (2007) found good agreement in 550 nm single scattering albedo, with differences between in situ measurements and AERONET retrievals of −0.01. In the mid-Atlantic region of the United States for weakly absorbing anthropogenic fine mode dominated aerosol, Schafer et al. (2014) found excellent agreement between aircraft vertical profiled in situ measurements of single scattering albedo (550 nm) and AERONET retrieved values (estimated at 550 nm from the mean of 440 and 675 nm values), with an average difference of only ~0.01 for spatially and temporally matched observations. Johnson et al. (2009) compared in situ measured aerosol optical properties from an aircraft vertical profile flight over the Banizoumbou (Niger) AERONET site on 19 January 2006. This was a mixed aerosol case with Angstrom Exponent (450–700 nm) of ~0.8–0.9 and high 550 nm AOD of ~0.75, where a shallow dust layer up to 1 km altitude was overlain by a layer of predominantly fine mode smoke. Both aircraft and AERONET measurements of column integrated AOD at 550 nm were in good agreement for this case, suggesting that both were sampling the same aerosol mixture. The aircraft measured column-mean SSA at 550 nm (from Particle Soot Absorption Photometer (PSAP) and nephelometer) was 0.87, in good agreement with the AERONET retrieval of 0.85 (interpolated to 550 nm). Toledano et al (2011) presented a comparison for a single dust aerosol case of spectrally measured in situ SSA versus an AERONET retrieval at Praia, Cape Verde showing differences of less than 0.02 at all four wavelengths from 440 nm to 1020 nm. Additionally, analysis by Eck at al. (2010) suggested that the difference between the AERONET retrieval climatology and DABEX in situ measured SSA at 550 nm (Johnson et al., 2008) would be ~0.02 or less (after accounting for in situ biases) over the measured range of scattering Angstrom exponents from ~0.1 to ~1.5. These offsets in SSA are smaller than the nominal ~0.03

https://doi.org/10.5194/egusphere-2026-5531
Preprint. Discussion started: 18 September 2026




uncertainty of AERONET at AOD(440) of 0.40 (Sinyuk et al., 2020). Additionally Sinyuk et al. (2020) show that the SSA uncertainty decreases substantially as AOD increases to values higher that 0.4 at 440 nm. We make further comparisons of dust aerosol spectral SSA obtained from retrievals by AERONET versus in situ laboratory measurements of dust generated from regional soil samples of spectral SSA in Section 3.2.1 below.

## 3. Results

### 3.1 Individual dust retrieval and examination of cross-Atlantic transport events

Before starting our multi-year database analysis it is beneficial to first analyze individual cases in detail to better understand the retrieved dust parameters from AERONET data: a) a single retrieval in Banizoumbou, Niger, in the Sahel region of West Africa at (Lat 13.55° N, Long 2.67° E) in Niger, b) the June 2020 Godzilla long range dust transport event from the Sahara/Sahel across to the Caribbean, and c) another trans-Atlantic dust transport event in 2023. These illustrate common variabilities in dust optical properties in these regions and also typical characteristics of the AERONET retrievals. To reiterate Level 2 retrievals are used (unless otherwise noted) meaning they passed all cloud screening, quality control, and retrieval fit checks for both spectral AOD and sky radiances (Giles et al. (2019); Sinyuk et al. (2020); Holben et al. (2006)). For all of these cases the aerosol loading was high (AOD(440) ranging from ~0.7 to 3.5) and the $AE_{440-870}$ was low <0.2 thus indicative of optical dominance by large size dust particles.

#### 3.1.1 Banizoumbou: An example of a single retrieval

The Banizoumbou site in the Sahel region in Niger is one of the longest sustained/historical benchmark AERONET sites for dust activity in the Sahel, and on March 13, 2022 experienced its most significant event since the site was updated to 1640 nm measurement capability in 2021. During this particular month three major dust events occurred with $AOD_{440}$>3 ($13^{th}$, 17th, and $24^{th}$) and with L2 retrievals. The retrieved aerosol volume size distribution (VSD) for the March 13 8:20 UTC case is shown in **Figure 2a**. Dominant in the volume size distribution is the familiar coarse mode peak with a modal radius of 2.3 µm and a geometric standard deviation of 1.4. This narrowness of the distribution may in part be influenced by reduced sensitivity of the retrievals to giant particles although those might be best treated in observations and modeling as a separate mode (e.g., Reid et al., 2006; 2008). Indeed, It is noted that the AERONET retrievals of dust size distributions have been shown to have reduced sensitivity to large or giant-sized dust particles with radius >10 micron (Ryder et al. 2015; Zheng et al. 2024). This is mainly due to these large dust particles having reduced optical effects in AERONET wavelengths compared to the other size ranges plus a retrieval upper radius limit of 15 µm. For example, Li et al. (2025) computed dust optical depth in the mid-visible (0.44-0.63 µm) to be insignificant for giant particles of radius greater than 10 µm. Furthermore, large and giant-sized dust particles are also significantly depleted with aging/transport due primarily to significant gravitational sedimentation (Formenti and DiBiago, 2024; Ryder et al. 2013), somewhat reducing their impact with distance from the source regions. In this paper our primary focus regarding retrieved size distributions is on the middle mode of sub-micron radius dust particles.

https://doi.org/10.5194/egusphere-2026-5531
Preprint. Discussion started: 18 September 2026




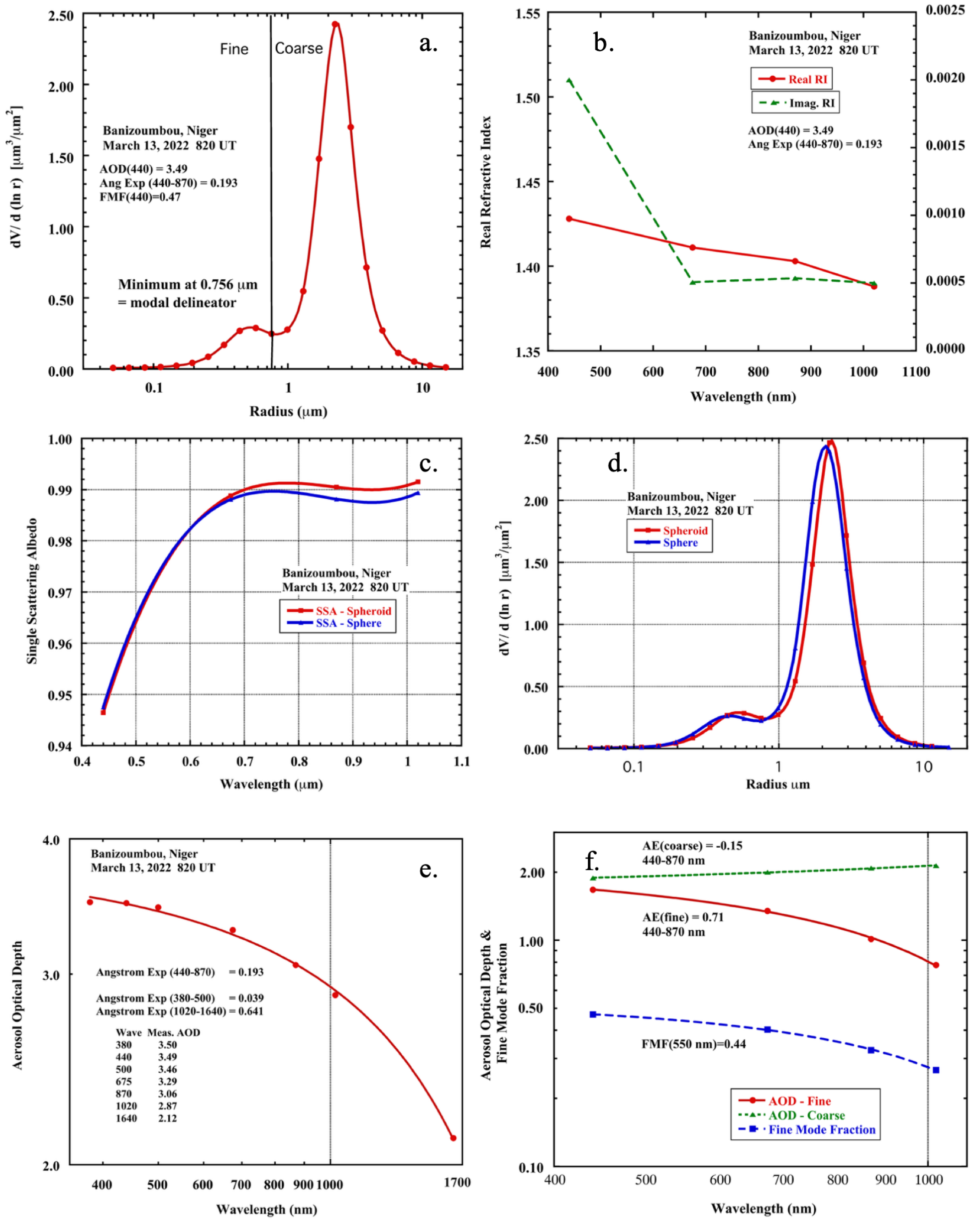


**Figure 2. AERONET L2 retrieval of (a) aerosol volume size distribution and (b) complex refractive indices from an almucantar sky scan at Banizoumbou, Niger on March 13, 2022 at 820 UTC. The AOD at 440 nm was 3.49 and the AE(440-870)=0.193. The fine-coarse mode radius delimiter was 0.756 mm, the local minimum between modes. Retrieved spectral single scattering albedo (c) for both the spherical and spheroid particle shape assumption. Aerosol size distributions (d) for both the spherical and spheroid particle shape assumption. Direct sun measured AOD spectra (e) from 380 to 1640 nm coincident in time with this Banizoumbou March 13, 2022 almucantar retrieval. (f) Retrieval computed fine and coarse mode AOD for the four input wavelengths with associated AE(coarse) of -0.15 and AE(fine) of 0.71. The FMF of AOD was computed to be 0.47 at 440 nm and 0.44 at 550 nm.**

https://doi.org/10.5194/egusphere-2026-5531
Preprint. Discussion started: 18 September 2026




While a dominant volume coarse mode exists at ~2.5 μm in radii for this case, also notable is a smaller, middle or shoulder mode, with a median diameter of ~0.55 μm. Such a "middle" mode is somewhat problematic, as it straddles the more common definition of fine mode particle with radii <0.5 μm typically associated with anthropogenic and biogenic particles. However, as discussed below such "middle" or intermediate modes are commonplace in dust and volcanic plumes; too large to be considered "fine" but also quite distinct from the dominant coarse or common mode typically associated with airborne dust. The AERONET algorithm automatically delineates fine versus coarse mode in the size distribution when there is a local minimum between 0.44 μm radius and 0.99 μm radius. As only two modes are defined if there is a middle mode or wide shoulder of the super-micron mode present then it is typically split between the fine and coarse modes. In this example case the local minimum volume concentration occurred at the radius of 0.756 μm, as shown in **Fig. 2a**. When there is no local minimum between this radius range then the fine/coarse mode cutoff is set at 0.44 μm, therefore splitting this middle mode into contributions to both the fine and coarse modes. Such a split then requires some caution in the analysis of AERONET modal size distribution products.

Other studies over the years have also noted the presence of these middle mode size particles in AERONET retrievals of dust dominated size distributions (Tanre et al. (2001); Todd et al. (2007); Eck et al. (2010); Gianelli et al. (2013); Torres and Fuertes (2021)). In situ observations have also been long supportive of not only dust in this size range, but also changes in minerology (Gomes et al 1990; Reid et al., 2003a; Reid et al., 2003b, Reid, E. A. et al. 2003; Reid et al. 2008). While a small fraction of total dust volume, it is nevertheless has also been long recognized as an important factor in Particulate Matter of aerodynamic diameter less the 2.5 mm ($PM_{2.5}$; e.g., Husar et al., 1998; Malm et al. 2004). Given its size relative to size parameter, these particles also have an amplified influence (i.e., maximum $Q_{ext}$=4) in visible wavelengths and are included in common aerosol models (Hess et al., 1998).

The retrieved refractive indices for this case are shown in **Figure 2b** where the imaginary refractive index (IRI) is nearly constant and low from 1020 nm to 675 nm at ~0.0005, while at 440 nm the IRI increases significantly to 0.002, long identified as indicative of the iron oxide content of mineral dust (Sokolik and Toon, 1999; Cattrall et al., 2003; Alfaro et al., 2004). While retrievals at additional wavelengths would certainly be useful, serendipitously, the absorption for hematite begins to increase significantly at wavelengths shorter than 650 nm, and hence the interpolation is likely good to first order (e.g. Marusak et al., 1980; Sokolik et al., 1993). We further discuss wavelength interpolation of SSA using AERONET retrieval wavelengths in section 3.2.1.

The complex refractive index and particle size distribution are then related to spectral SSA, for this case is shown in **Figure 2c** using both the standard V3 retrieval (spheroidal shape) and for the retrieval made with spherical shape assumption. This retrieval is also consistent with observations; Di Biagio et al (2019) measured the iron oxide content of dust generated from desert soil samples obtained throughout the world and also measured the dust single scattering albedo (SSA) in a laboratory smog chamber. They showed a strong correlation between short wavelength (370 nm) SSA and iron oxide percentage while at the long wavelength of 950 nm there was very little variation of

https://doi.org/10.5194/egusphere-2026-5531
Preprint. Discussion started: 18 September 2026




SSA as a function of iron oxide content and all SSA values were high at 950 nm. It is noted that the shape assumption (spheroidal versus spherical) has a very minor effect on the SSA retrieval for all dust case retrievals (**Figure 2c**). Similarly, the particle shape assumption has a minor effect on retrieved size distribution for this high AOD case (**Figure 2d**). That is due to the multiple scattering at very high AOD reducing the influence of particle shape in the retrieval. It is noted that for low to moderate AOD dust case retrievals the spherical particle shape assumption results in large anomalies in fine mode size distribution and in the real part of the refractive index (Dubovik et al., 2006; Eck et al; 2005). However, these significant anomalies counter each other in the computation of SSA thereby resulting in minor SSA differences as compared to retrievals made with the spheroidal particle shape assumption. The AERONET retrieved real refractive index for this case varied from 1.43 at 440 nm to 1.39 at 1020 nm. All three major high AOD dust events in Banizoumbou in March 2022 provided similar values to +/-0.01. However, the retrieval of the real part has the least sensitivity in the AERONET inversion (Sinyuk et al., 2020).

The AOD spectra from 380 to 1640 nm associated with this almucantar retrieval is shown in **Figure 2e**. Note that only the 440, 675, 870 and 1020 nm AOD along with sky radiance distributions for these same four wavelengths were utilized as input to the V3 retrievals. There is significant decline in AOD at 1020 nm and especially 1640 nm in this case. Consequently, the Angstrom Exponent increased significantly as wavelength increased ranging from ~0.04 at 380-500 nm to ~0.64 at 1020-1640 nm. The computed AOD spectra from the retrieval for the fine mode (radius <0.756 μm) and coarse mode separately are shown in **Figure 2f**, where the coarse mode AE(440-870) was -0.15 while the AE for the sub-micron mode was 0.71. Also shown in **Figure 2f** is the fine mode fraction (FMF) of AOD which was 0.47 at 440 nm and 0.44 at 550 nm. This might initially seem to be a high FMF of AOD in the visible wavelengths for a case with AE(440-870) of 0.193, however we later show that it is somewhat typical since middle mode sized particles are widespread and essentially ubiquitous in the Sahel/Sahara region.

### 3.1.2 Long range transport events.

In comparison to the March 2022 Banizoumbou case study, it is also helpful to demonstrate the nature of retrievals for major dust transport events. First, the so-called "Godzilla" dust event is highly noteworthy as the largest transatlantic dust event in over a generation (Yu et al. 2021). AERONET retrievals made on opposite sides of the Atlantic Ocean are compared in Figure 3. **Figure 3a** shows the normalized (to peak value) size distributions of retrievals made at two AERONET sites on and near to the west coast of Africa (Dakar_Belair and Capo_Verde) and also at four sites in the Caribbean region (Ragged Point, La Parguera, Cape San Juan, and Guadaloup) during this major dust event. The AOD(440) was high for these retrievals at all of these sites/dates ranging from 3.16 at Capo Verde to 1.31 at Ragged Point while all retrievals had very low AE(440-870) ranging from 0.04 to 0.11, thereby confirming dust dominance in the total atmospheric column. Note that while back trajectories show that the dust over the Dakar_Belair did not advect to the Caribbean region (however dust over Cape Verde did) the aerosol properties at this site are nonetheless associated with this massive historic transport event. While all retrievals showed a significant 'middle mode', the two retrievals near the coast of Africa show relatively less contribution of the middle mode size (radius < 1 micron) as compared to the retrievals at four sites in the Caribbean after cross-Atlantic transport. This is consistent with larger dust particles possibly being preferentially removed by sedimentation during this trans-Atlantic transport event. High $PM_{2.5}$ levels were measured in the Caribbean and

https://doi.org/10.5194/egusphere-2026-5531
Preprint. Discussion started: 18 September 2026




Yucatan Peninsula, Mexico during the Godzilla event (Mayol-Bracero et al., 2025) thereby consistent with the significant middle sized particle mode inferred by AERONET.

Also noteworthy regarding the middle mode was that the Capo Verde retrieval of the FMF of AOD(440) was 42% while the other retrievals did not have a local minimum and therefore the fine mode calculation did not include the entire middle mode sized contribution. The very low AE(440-870) values (0.04 to 0.11) for all of these retrievals indicates that the AE of the middle mode is quite low since the AE of coarse mode only particles is approximately -0.15. Assuming that total AE is a linear weighted value by fine mode fraction of AOD of the coarse and middle modes (O'Neill et al., 2001; equation 4) then for a total AE of 0.07 and 40% of total AOD in the middle mode, the computed AE(440-870) of the fine mode fraction which in this case is dominated by the middle mode would be 0.40.

Additionally noteworthy is the perceived changes in single scattering albedo with transport. **Figure 3b** shows the retrievals of SSA for these same sites/dates. The SSA at 440 nm were higher (~0.925 to 0.94) at 440 nm for the four Caribbean site cases as compared to the two sites on or near the coast of West Africa where SSA at 440 nm was ~0.88 to 0.905. For a given set of complex refractive indices, SSA typically goes up for smaller relative size; there is simply less material in a particle to absorb and additionally increasing refraction. Therefore given the relative increase in volume of the middle mode, the SSA would be expected to increase. However, it cannot be ruled out that different portions of this major dust plume had somewhat differing amount of iron oxides in the mineral aerosols leading to differing magnitudes of absorption in space and time, plus the likely interaction of sea salt and dust aerosol in the boundary layer in the Caribbean (Sherstra et al., 2025) which may potentially create hygroscopic dust.

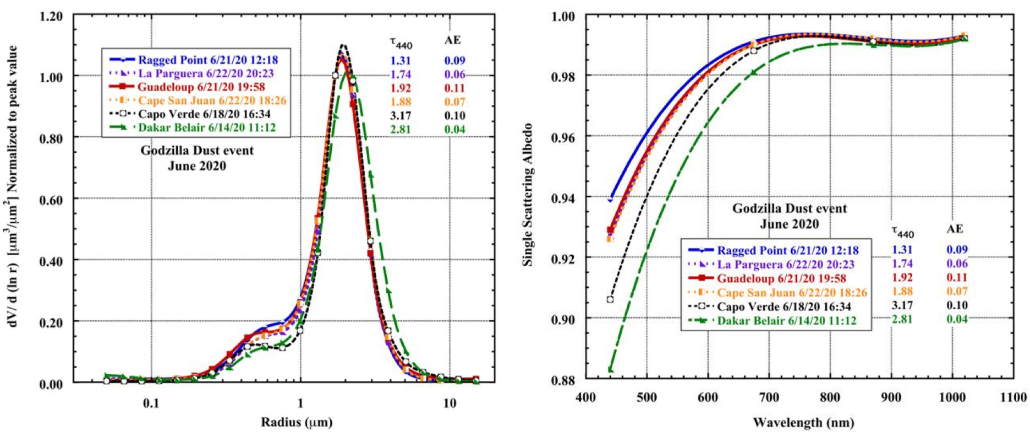


**Figure 3. AERONET retrieved size distributions (a) and single scattering albedo spectra (b) during the major Saharan dust event from June 14 – 22, 2020 called the 'Godzilla' event. Five sites in the Caribbean region and two near or at the coast of West Africa are shown for this trans-Atlantic dust transport event. All retrievals are L2 except the L1.5 Capo Verde retrieval which had SZA=43 therefore below the threshold of 50 degrees. Very high AOD for this Capo Verde data however increases the aerosol sensitivity and significantly reduces the uncertainty of this case.**

https://doi.org/10.5194/egusphere-2026-5531
Preprint. Discussion started: 18 September 2026




The second large trans-Atlantic transport event that we examine here occurred from 11-15 August, 2023 that was documented in Reid et al. (2026). The AOD(440) was high at 0.68 to 0.81 for all sites examined here and the AE(440-870) was very low at 0.05 to 0.14 thus consistent with a coarse mode dominated dust event. For this dust transport event we did not normalize the size distribution retrievals since the AOD was nearly the same for all the sites/cases compared. The 'middle mode' was similar in magnitude for observations both near to Africa and at Barbados (Ragged Point) for this case (**Figure 4a**). The lack of change in volume dust size distributions for sites near the African continent versus in the Caribbean basin is somewhat consistent with the analysis of Maring et al. (2003) who measured similar volume size distributions in the Canary Islands and Puerto Rico except for particles of radius greater than 7.3 microns. They attributed the lower volume of the largest particles in Puerto Rico to likely be the result of gravitational settling over the ocean. As noted previously the weak sensitivity of AERONET optical measurements to these large-size dust particles limits the ability of these retrievals to detect changes in the size distributions of the largest dust particles in the coarse mode. The 440 nm SSA was higher at Ragged Point by ~0.02 as compared to the Roque Muchachos site (**Figure 4b**). Note that the Roque Muchachos site is at much higher altitude in the Canary Islands, 2396 m versus 52 meters for the Santa Cruz Tenerife site. This suggests possible differences in SSA with altitude nearer to the source regions, or alternatively possibly due to spatial/temporal variation in dust properties since the dates also differ. In the following sections we include multi-year statistical comparisons of retrieved size distributions and SSA from the Ragged Point (Barbados) site to the Cape Verde site, located on opposite sides of the Atlantic Ocean.

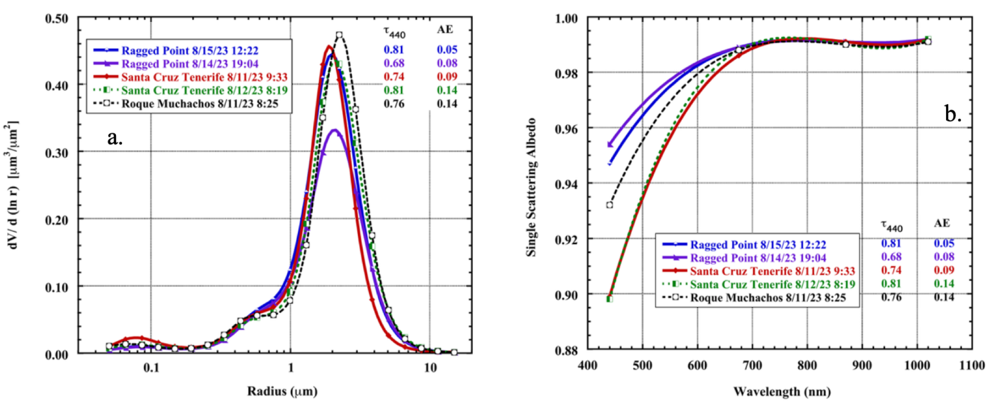


**Figure 4. AERONET retrieved size distributions (a) and single scattering albedo spectra (b) during a major Saharan trans-Atlantic transport dust event from August 11-15, 2023. All are L2 retrievals from one site in the Caribbean and two sites near West Africa in the Canary Islands.**

## <u>3.2 Multi-year monitoring of dust optical and physical properties</u>

In this section we primarily examine multi-year data sets obtained from AERONET monitoring for selected sites located in and downwind of major dust source regions over time intervals of ~15 to 24 years. The sites with largest statistical sample size of AERONET dust AOD dominated retrievals were five sites in the Sahel/Saharan region or immediately downwind and one site in the Arabian Peninsula (e.g. see Figure 1). The high measured AOD

https://doi.org/10.5194/egusphere-2026-5531
Preprint. Discussion started: 18 September 2026




at these sites is consistent with global maps of these same regions showing modeled high dust emission (Goncalves Ageitos et al., 2023), modeled high dust AOD in the mid-visible (Ginoux et al. 2001; Leung et al., 2025) and regions of satellite-measured large magnitude dust AOD (Song et al., 2021) or Aerosol Index (Herman et al., 1997). All of these analyses showed high dust emission and high AOD in the extensive regions of the Sahara/Sahel and Middle East/ Arabian Peninsula, yet much lower AOD in most other global dust source regions. These AERONET sites with high AOD (>0.4 at 440 nm plus low AE<0.4 at 440-870 nm) had from 1156 to ~4100 retrievals each thereby providing robust dust characterization of single scattering albedo and size distributions. We only utilized almucantar scan retrievals for these multi-year analyses since hybrid scan retrievals were only available for a varying fraction of the total years at each site depending on when the latest model-T Cimels were operating there. Additionally in the early mornings and late afternoons there were both hybrid and almucantar scans made within ~12 minutes of each other and therefore essentially double sampling the same conditions given the excellent agreement between these two scan types when closely matched in time (Sinyuk et al., 2020).

Desert regions typically have much lower cloud fraction than most other regions, thus sky conditions are favorable for both AERONET retrievals and for AOD to pass cloud screening and quality checking to reach level 2. Three other sites we analyzed had far fewer retrievals that met the AOD(440)>0.4 and AE<0.4 thresholds, ranging from 25 to 92 per site despite long-term monitoring at all sites. These sites were located in the Caribbean (Ragged Point, Barbados), Australia (Birdsville) and the Gobi Desert (Dalanzagad) and the small sample sizes there were also consistent with much lower dust AOD in these dust source or receptor regions as compared to the Sahara/Sahel and Saudi Arabian Peninsula (Leung et al., 2025; Song et al., 2021; Kok et al., 2021). In order to focus on dust dominated retrievals of aerosol optical properties we only analyzed retrievals where the Angstrom Exponent from 440-870 nm (AE(440-870)) was less than 0.4. These are cases where the coarse mode typically exceeds the fine mode mid-visible AOD. For example, Eck et al. (2010) show that retrieval derived fine mode fraction of AOD at 500 nm is ~35% at AE(440-870)=0.4. Here the fine mode AOD was defined differently by the Dubovik algorithm that employs a radius cutoff and from the Spectral Deconvolution Algorithm (SDA; O'Neill et al., 2003) where the fine / coarse mode distinction is entirely optical (see Section 2 of O'Neill et al., 2023). Additionally both the Dubovik and SDA algorithms define only two particle size modes therefore are not rigorous modal classifications when three modes occur. When a trimodal distribution occurs the middle mode is typically split by both algorithms with fractional contributions to the two modes (fine and coarse). The definition of fine mode particle size is not a universally defined and accepted value and has significant range. Therefore, the FMF of AOD for low AE observations can show significant variation dependent on the definition applied. Additionally, we analyze data where AOD(440) exceeded 0.40 in order to reduce uncertainty in retrieved single scattering albedo to 0.03 or even less at higher AOD (Sinyuk et al., 2020).

https://doi.org/10.5194/egusphere-2026-5531
Preprint. Discussion started: 18 September 2026




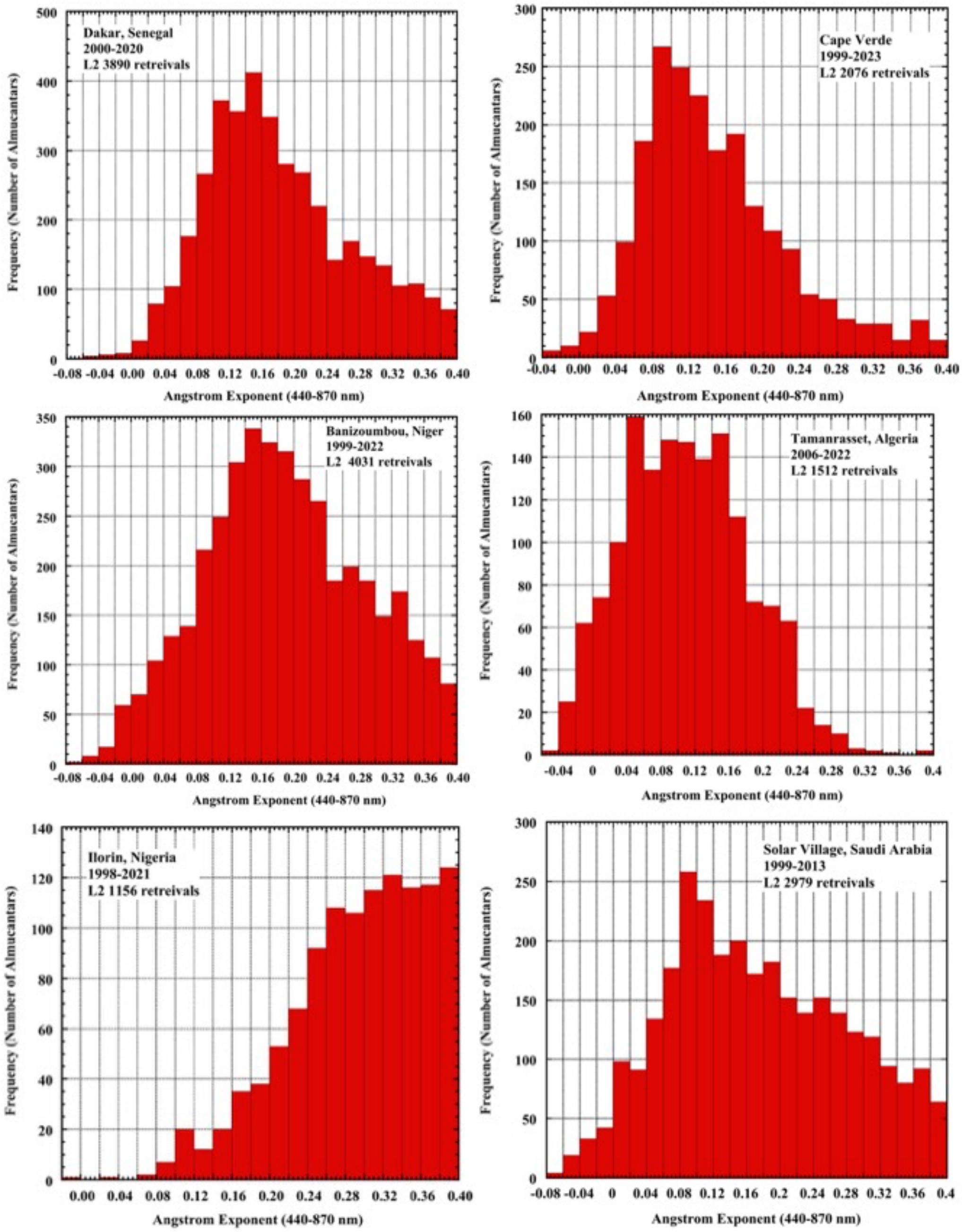


**Figure 5. Histograms of AE(440-870 nm) for five sites in the Sahel, Sahara and near the coast of West Africa plus one site in the Saudi Arabian Peninsula from climatological multi-year monitoring for L2 almucantar retrievals with AOD(440)>0.4 and AE(440-870)<0.4. AE computed from direct sun measured AOD.**

https://doi.org/10.5194/egusphere-2026-5531
Preprint. Discussion started: 18 September 2026




We begin our global dust characterization with **Figure 5** that shows the histograms of AE for all retrievals with AOD>0.4 (for suitable refractive index retrievals) and AE<0.4 (identifying coarse mode dominated) for the five sites in the Sahel and Saharan regions plus the one site in the Saudi Arabian Peninsula (Solar Village) – regions which include the world's largest dust sources. For two sites in the Sahel (Banizoumbou and Dakar) the histogram peaked at ~0.10 to 0.16 while showing very few retrievals with negative AE and a skewed tail of decreasing frequency as AE increased past the peak frequency. Likewise for Cabo Verde just offshore in the Atlantic, AE diminished further, with a modal value of 0.09. For the one site within the Sahara (Tamanrasset), the histogram is narrower still with peak frequencies from AE ~0.04 to 0.16 and with very few values with AE>0.26. For the Solar Village site the histogram of AE is similar to that of the Dakar site. For the site that is the farthest south and also located in a large city (Ilorin, Nigeria; pop. ~1.5 million metropolitan region) the AE histogram is different from the others with a very broad range of highest values from AE of ~0.30 to 0.40. This is very likely mostly due to mixing of desert dust with fine mode urban/industrial pollution, more biomass burning aerosol (higher rainfall in this greater vegetation density region) and additionally possibly due to being downwind from (and the closest AERONET site) to a unique major dust source, the Bodele Depression with somewhat different source material of diatomaceous sediment plus fish bone and scale (Hudson-Edwards et al., 2014) since it is the site of an ancient dried lake bed (Drake et al., 2022), or other parts of the Sahara that are known for higher prevalence of more broadly absorbing goethite (Go et al. 2022). Even the Tamanrasset site occasionally sees petrochemical influence from Libya (Guiardo et al. 2014). Note that the Dakar AERONET site is located ~65 km southwest of the city of Dakar and therefore the urban/industrial pollution from that city has minimal impact on that AERONET site.

Another aspect of AERONET dust retrievals is particle sphericity. The AERONET retrieval algorithm selects the percentage of spherical versus spheroidal shaped particles that results in the best fit to the measured sky radiances (Dubovik et al, 2006). For the data analyzed in this paper the applied threshold of AE(440-870)<0.4 plus all sites being located in major deserts and/or downwind of dust source regions resulted in the percentage of spheroidal particles in the almucantar retrievals that was typically > 95% and for the vast majority of cases >98%. This is further evidence of these cases being dust dominated since the spheroidal particle assumption fits the angular sky radiance distribution better for non-spherical desert dust particles (Dubovik et al., 2006).

The magnitudes and seasonality of AOD utilized in the retrievals show significant variability throughout the annual cycle. The 440 and 675 nm AOD data as a function of the day of year for three sites, Dakar, Tamanrasset and Ilorin are shown in **Figure 6**. For Dakar and Tamanrasset it is notable that there are fewer dust event cases that meet these criteria for November through February. Therefore, for most of the northern hemisphere late fall and winter months there were few moderate to strong dust dominated events in this region. This may be due in part to extensive biomass burning in this west African region that occurs from November through February (N'Datchoh et al., 2015) therefore resulting in values of AE above the maximum threshold of 0.4. Conversely, for the Ilorin site there were more strong dust events in the late fall to early spring seasons. This is notable in relation to higher seasonal prevalence then of nocturnal jet dust production around the nearest source the Bodele depression (e.g., Fiedler et al., 2013) plus northwesterly winds. At the same time, biomass burning in the Sahel also peaks in winter (Duncan et al. 2003; Ichoku et al. 2016), leading to potential dust-smoke and regional pollution mixtures. For the boreal summer

https://doi.org/10.5194/egusphere-2026-5531
Preprint. Discussion started: 18 September 2026




months at Ilorin, winds shift to southwesterly with the arrival of the monsoon and associated heavy cloud cover and rainfall.

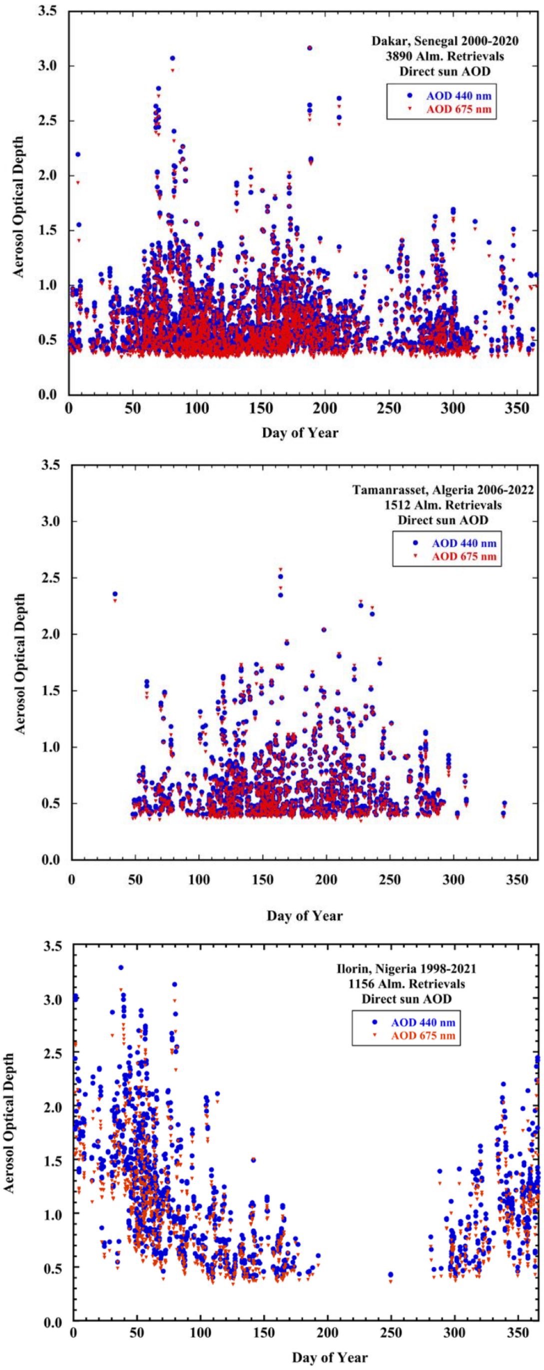

**Figure 6. AOD at 440 nm and 675 nm versus day of year from climatological multi-year monitoring for L2 almucantar retrievals with AOD(440)>0.4 and AE(440-870)<0.4.**

The maximum AOD that occurred with a successful AERONET retrieval at any site was AOD(440)~3.5. An examination of the maximum dust case AOD for direct sun data only without an associated inversion was similar at ~3.7 at 440 nm. This contrasts with maximum AOD measured for biomass burning events by AERONET sun-sky radiometers at much higher levels. Giles et al. (2019) computed a maximum AOD value of 7.3/m (m = optical airmass) based on the minimum signal allowed in AERONET quality control in order to eliminate falsely low values due to diffuse radiation in the instrument FOV (Sinyuk et al. 2012). Eck et al. (2019) reported measurements of Indonesian smoke AOD at 675 nm to a maximum of 7.1. However, the AERONET triplet variability check (AOD range of 3 measurements taken 30 sec apart) for temporal variance is only applied to the 675, 870 and 1020 nm channels and therefore allows much greater high frequency variation in the shorter wavelengths where the AOD is much higher and more variable for fine mode dominated aerosol. Note that all three of these wavelengths must have triplet variability that exceeds the threshold before the AOD are screened as cloud contaminated. Moreover, the cloud screening and quality control algorithms developed by AERONET team and described by Giles et al. (2019) allow for the restoration of high AOD cases that also have high AE(675 to 1020 nm) >1.2, therefore are fine mode dominated cases. There is no such restoration of high AOD cases for dust dominated coarse mode aerosol since the low AE at very high optical depths could be due to either dust and/or cloud contamination. Therefore, it is virtually certain that there were extreme dust events with AOD >3.7/m that were screened by the AERONET algorithms due to a combination of cloud screening checks on temporal variance and other quality control thresholds including low direct sun signal thresholds.

The following subsections each focus on a single retrieved or measured parameter from the AERONET database for the nine primary sites mentioned above, utilizing the data obtained from extensive multi-year monitoring at each site.

### 3.2.1 Single Scattering Albedo (SSA)

Spectral SSA retrievals from AERONET sky radiance scans are quite robust due to several factors. First, the retrieved size distributions and complex refractive indices are utilized to compute the extinction AOD and these spectral values match the direct sun measurements of spectral AOD to within 0.01, which is the accuracy of the measured AOD at airmass of 1 for visible and near-infrared channels (Eck et al., 1999). Therefore, the high accuracy of the direct sun measured extinction AOD ensures that the retrieved total extinction is robust. Second, both the retrieved size distribution and the real part of the refractive index are the parameters that describe the scattering by the total column aerosol, while only the imaginary part describes the absorption. Therefore, if there is a bias in retrieved size distribution or real refractive index then this is compensated by an offset in the other scattering parameter, thereby together providing a close agreement with the measured scattered radiation (Sinyuk et al., 2020). Furthermore, an independent retrieval developed by co-author Alexander Sinyuk called the ‘alternative retrieval’ utilizes the same input data (spectral AOD and directional sky radiances) but retrieves only two parameters: the

https://doi.org/10.5194/egusphere-2026-5531
Preprint. Discussion started: 18 September 2026




spectral SSA and spectral scattering phase function. The size distribution is not retrieved or assumed and there is no assumption or model applied for the particle shape in this alternative retrieval. This retrieval has been utilized in several test cases (unpublished) at moderate to high AOD and these cases have shown very close agreement (typically <0.01) in retrieved SSA with the current AERONET V3 algorithm retrieval. Also since the constraint on the spectral variation of the imaginary refractive index is already relaxed in these V3 retrievals at low AE for dust cases, there will be little change in SSA retrieved in the future V4 inversion algorithm (see Sinyuk et al., 2022). Additionally, the average 440 nm AOD of the dust cases for these multi-year means of SSA are high ranging from ~0.50 (at Birdsville) to 1.18 (at Ilorin). The average AOD(440) for the other Sahel and Saharan sites plus the Saudi Arabian and Gobi sites range from 0.63 to 0.78. The relatively high aerosol loadings for the retrieval datasets presented here results in relatively low SSA uncertainty (Sinyuk et al., 2020). Therefore from Figure 22 in Sinyuk et al. (2020) for the Mezaira (UAE) dust aerosol site the average estimated uncertainty in the SSA retrievals for all four wavelengths ranges from ~0.01 for the highest AOD site to ~0.02 for the lowest AOD site in the current dust aerosol study.

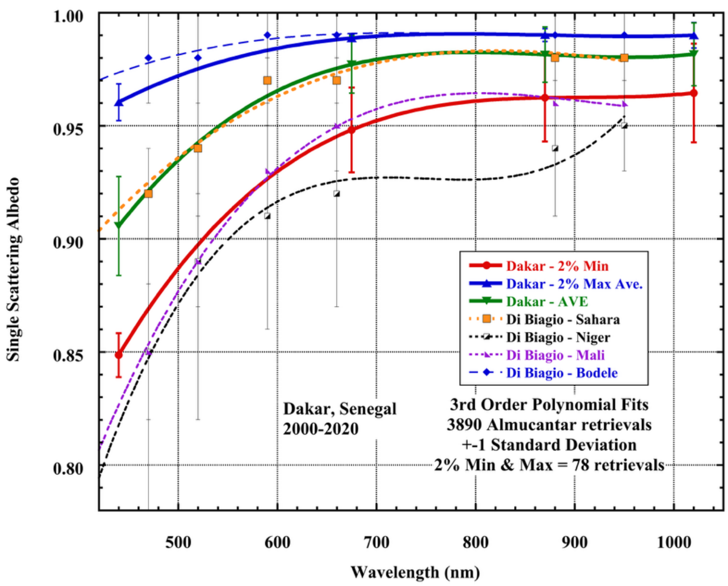


**Figure 7. Spectral SSA from AERONET almucantar retrievals at the Dakar, Senegal site showing climatological averages plus averages of the highest 2% and lowest 2% of retrieved SSA values. The spectral SSA of laboratory generated dust from soil samples of Di Biagio et al. (2019) are also shown for the Saharan region sample average and for specific high and low SSA sample sites in the Sahel. The curve fits for both the AERONET and DB19 spectral variation of SSA are third order polynomials. Bars depict plus and minus one standard deviation values.**

Multi-year statistical data of AERONET retrievals of SSA (means & standard deviations) were compared to dust from soil sample suspensions in a lab chamber by Di Biagio et al. (2019) hereafter DB19. It is noted that the DB19 measurements are the only other dust spectral SSA database (other than AERONET) representing a sampling of all major dust source regions on the planet. Spectral mean retrieved SSA in the Sahel and Sahara region agree

https://doi.org/10.5194/egusphere-2026-5531
Preprint. Discussion started: 18 September 2026




very well with Sahara means from DB19. For example, the comparison of AERONET retrieved SSA at the Dakar site to the DB19 data are shown in **Figure 7**. Third order polynomial fits to all wavelengths of the spectral SSA data from both AERONET and DB19 are shown. These 3rd order fits are excellent fits to within <0.01 to both the AERONET SSA spectral values from 440 nm to 1020 nm and also to the DB19 data from 370 nm to 970 nm. Additionally, these spectral fits show good SSA agreement (within 0.01 or less for all wavelengths) for the overall mean of 3890 Level 2 retrievals at Dakar as compared to the Sahara region average of DB19, which includes values from five different Saharan soil sample locations. Extremes defined from the two standard deviation tails (highest and lowest 2% of all 440 nm SSA retrieved values) of the SSA retrieval database from the AERONET Dakar site also agreed with the least absorbing soil sample in the region (Bodele) within less than 0.015 and the agreement with the most absorbing soil samples in the Sahel region (Mali and Niger) is within ~0.03 or less. The AERONET retrieved 440 nm SSA at each site are very close to normally distributed, justifying the 2% extremes as being representative of the two standard deviation tails. The SSA at all other AERONET wavelengths are not normally distributed but have a relatively narrow range of variability.

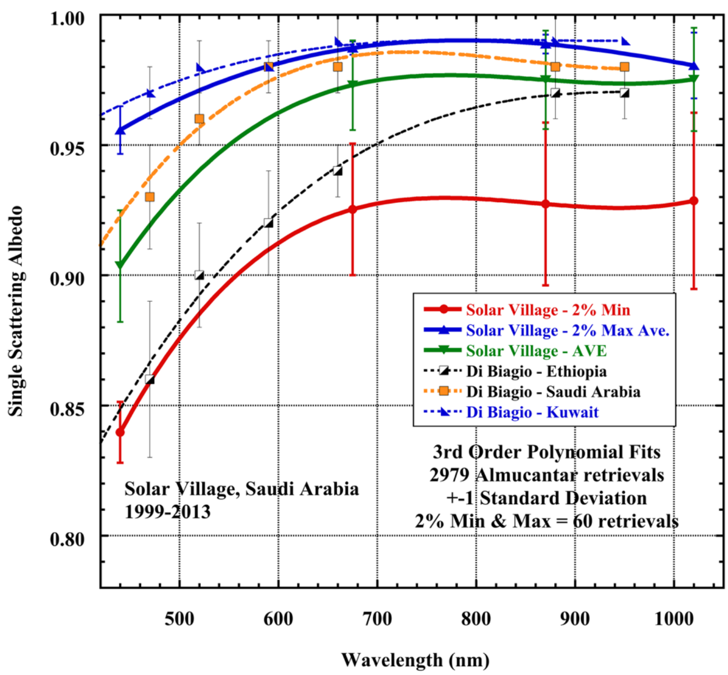


**Figure 8. Similar to Figure 7 but for the AERONET site at Solar Village, Saudi Arabia. The DB19 dust SSA were generated from soil samples collected in Saudi Arabia plus Kuwait and Ethiopia.**

Good agreement, of SSA within 0.02 or less, was also observed between the AERONET database of average SSA at Solar Village (Saudi Arabia) and the DB19 values for samples in the same source region (Arabian Peninsula), shown in **Figure 8**. There were nearly 3000 retrievals analyzed for the Solar Village site therefore the statistical sample is robust. Furthermore the 2% least absorbing SSA retrievals agreed to withing 0.01 or less with

https://doi.org/10.5194/egusphere-2026-5531
Preprint. Discussion started: 18 September 2026




the DB19 soil sample measurements from Kuwait. The 2% lowest SSA retrievals from Solar Village agreed well with the DB19 measurements from Ethiopia for the 440 nm and 675 nm wavelengths (within 0.02 or less), while for the longer wavelengths of 870 and 1020 nm the retrievals showed significantly lower SSA (~0.045) as compared to the Ethiopia soil sample values. For Australia there were very few retrievals (only 33) that met the AOD and AE criteria due primarily to typically low AOD at this site. However the lowest one sigma tail values (only 5 retrievals however) at Birdsville were very close to the single location DB19 soil sample values, within ~0.01 at all wavelengths. The average AERONET retrieved SSA was ~0.08 higher at the 440 nm and ~0.04 higher at the 675 nm wavelength, as compared to the DB19 soil sample. Large variability in soil color occurs in the vicinity of Birdsville, Australia (**Figure 9**). More red color is indicative of high iron oxide content while tan and brown soils indicate lower iron oxide content. Airborne soil dust at Birdsville could therefore be expected to have significant variation in absorption magnitude in short wavelengths, in part dependent on the erodibility of the different soil types. For the Gobi Desert in Asia there was good agreement between the AERONET average at Dalanzadgad (Mongolia) and the Gobi soil sample from DB, all wavelengths had SSA differences < 0.01. The lowest one standard deviation tail (16%) of SSA values from the 25 total retrievals (only 4 retrievals) agreed well with the DB19 soil sample values from the Taklimakan desert, within <0.02 at all wavelengths.

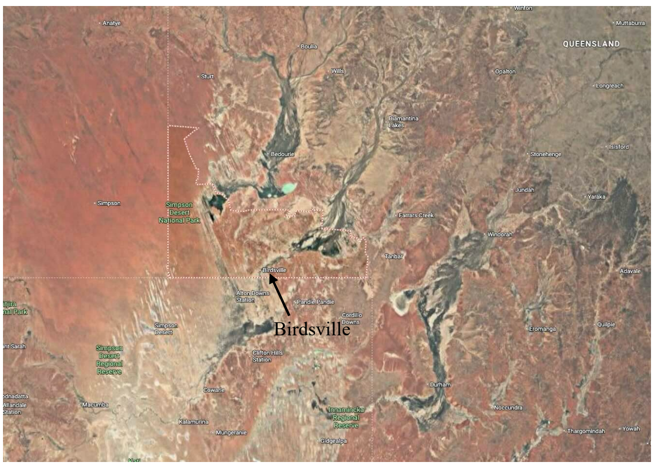


**Figure 9. Satellite image of the desert region in the vicinity of Birdsville, Australia (an AERONET site) showing the large variation of soil color. Imagery ©2026 NASA, Map data ©2026 Google.**

Comparisons of data from multi-year retrievals of SSA for dust at the Caribbean site of Ragged Point, in Barbados versus at Cape Verde off the coast of Africa were also examined (**Figure 10**). Both sites are islands in the Atlantic so both also have a background contribution of sea salt AOD to the total aerosol mixture. Average SSA and minimum SSA at Ragged Point, Barbados are significantly higher as compared to Cape Verde primarily at 440 nm, ~0.02 higher for the average and ~0.06 higher for the minimum subsets. The following are potential factors for these differences: (1) dust sources for the largest trans-Atlantic transport events may possibly have higher SSA therefore potential differences in the source regions for dust plumes measured at these two sites, (2) possible size distribution changes occur in trans-Atlantic transport, (3) the very small sample size of retrievals at Barbados (92) may not be

https://doi.org/10.5194/egusphere-2026-5531
Preprint. Discussion started: 18 September 2026




truly representative versus robust sample at Cape Verde (2076) and (4) potential changes to dust over time such as internal mixing with sea salt in the marine boundary layer which changed particle properties such as hygroscopicity at Barbados (Shrestha et al., 2025) and may also potentially reduce absorption.

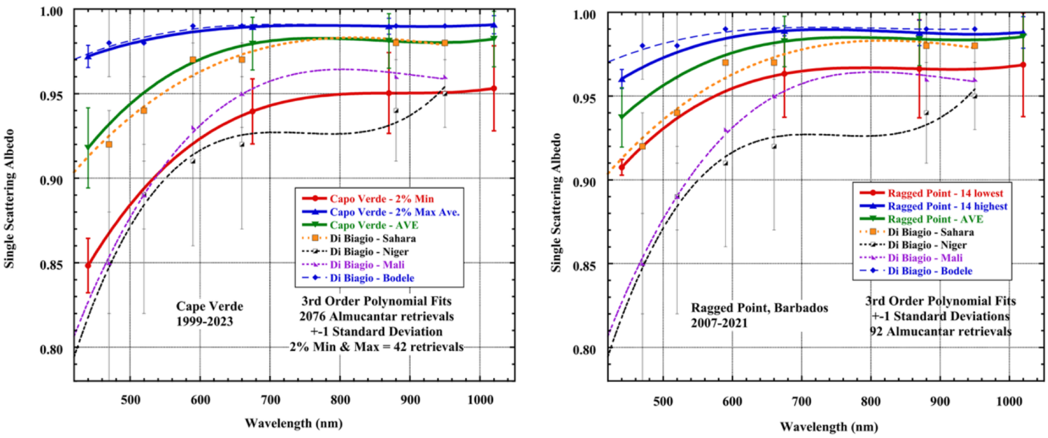


**Figure 10. Similar to Figure 7 but for two island sites on opposite sides of the Atlantic Ocean. Due to much smaller sample size of 92 almucantar retrievals for Ragged Point (right side panel) the 14 highest and lowest values (~1 standard deviation wings) are shown versus the 2% min and max values (2 standard deviation wings) for the Cape Verde site (2076 almucantars).**

Comparisons of the multi-year averages of spectral SSA for all the sites examined in detail in this study are shown in **Figure 11 and Table 1**. The sites include the five sites in the Sahel and Sahara, and single sites located in the western Atlantic (Caribbean Sea), the Saudi Arabian Peninsula, the Gobi Desert and in arid outback Australia. The SSA for all 5 sites in the Sahel and Sahara show similar spectral SSA within ~±0.01 of the five-site mean at 440 nm and less variation across sites at all the longer wavelengths (675 to 1020 nm). The 550 nm interpolated values of SSA from AERONET reported by Kim et al. (2011) for a smaller sample size, lower AE(440-870) threshold of <0.2, different database version and logarithmic interpolation between 440 and 675 nm are very similar to the 3$^{rd}$ order polynomial curve values for 550 nm in Figure 11 for the same sites. The 550 nm SSA values in Figure 11 are ~0.002 to ~0.01 higher than reported by Kim et al. (2011) depending on site. The average spectral SSA in Figure 11 at the Gobi Desert site (Dalanzadgad) and at the Saudi Arabian site (Solar Village) both had similar SSA magnitude to the five sites in the Sahel/Sahara. The SSA at the site in Australia (Birdsville) had the lowest average SSA, ~0.025 lower at 440 nm than the next lowest at Tamanrasset, Algeria in the Sahara. The Australia soil sample in DB19 also had the lowest measured SSA of all soil samples presented in that study. The site in the Caribbean (Ragged Point) had the highest AERONET retrieved spectral SSA values at all wavelengths, at 440 nm it was ~0.02 higher than the average at Cape Verde, which was the 2$^{nd}$ highest at 440 nm.

https://doi.org/10.5194/egusphere-2026-5531
Preprint. Discussion started: 18 September 2026




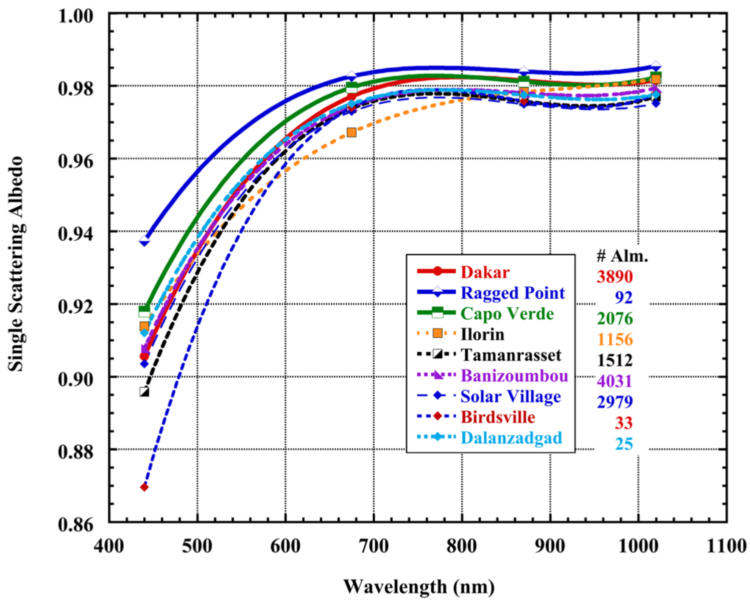


**Figure 11. Climatological averages of spectral SSA for nine sites with multi-year monitoring. Six sites have robust statistics with ~1100 to ~4000 almucantar retrievals averaged per site while the other three sites (Ragged Point, Birdsville and Dalanzadgad) have much smaller sample sizes due to AOD typically being much lower than the applied threshold of AOD(440)>0.4.**

**Table 1. Spectral Single Scattering Albedo (SSA) averages and standard deviations computed from multi-year monitoring at the nine primary sites for dust cases where AOD(440)>0.4 and AE<0.4. N is the number of almucantar scans.**

| Site | 440 nm SSA ave | 675 nm SSA ave | 870 nm SSA ave | 1020 nm SSA ave | 440 nm SSA std | 675 nm SSA std | 870 nm SSA std | 1020 nm SSA std | N |
|---|---|---|---|---|---|---|---|---|---|
| **Dakar** | 0.906 | 0.977 | 0.981 | 0.982 | 0.022 | 0.013 | 0.012 | 0.014 | 3890 |
| **Capo Verde** | 0.918 | 0.980 | 0.981 | 0.982 | 0.024 | 0.016 | 0.016 | 0.016 | 2076 |
| **Banizoumbou** | 0.908 | 0.974 | 0.978 | 0.979 | 0.025 | 0.018 | 0.018 | 0.019 | 4031 |
| **Tamanrasset** | 0.896 | 0.974 | 0.976 | 0.977 | 0.032 | 0.027 | 0.028 | 0.029 | 1512 |
| **Ilorin** | 0.914 | 0.967 | 0.978 | 0.982 | 0.023 | 0.016 | 0.014 | 0.014 | 1156 |
| **Solar Village** | 0.903 | 0.973 | 0.975 | 0.975 | 0.021 | 0.017 | 0.019 | 0.020 | 2979 |
| **Ragged Point** | 0.937 | 0.983 | 0.984 | 0.985 | 0.018 | 0.015 | 0.016 | 0.016 | 92 |
| **Birdsville** | 0.870 | 0.974 | 0.976 | 0.978 | 0.037 | 0.016 | 0.014 | 0.015 | 33 |
| **Dalanzadgad** | 0.912 | 0.975 | 0.977 | 0.978 | 0.019 | 0.013 | 0.013 | 0.015 | 25 |

Seasonal variation in SSA from the multi-year monitoring of dust cases were examined for sites in the Sahel and Sahara. At three sites (Ilorin, Dakar and Cape Verde) the SSA data at 440 nm showed similar seasonal cycles (although smaller in amplitude at Cape Verde). The maximum SSA occurred in July-August while the minimum was

https://doi.org/10.5194/egusphere-2026-5531
Preprint. Discussion started: 18 September 2026




in December-January for these sites. At Dakar the annual range in average SSA was ~0.04 at 440 nm with a minimum of ~0.885 and maximum of ~0.925 (**Figure 12a**). It is likely that there was some mixing and/or coating of dust with biomass burning aerosol in the months of November through February (days 300-365 and 1-60) since these are the months with maximum burned area in the Sahelian and Sudanian zones (N'Datchoh et al., 2015). However, the majority of the 440 nm SSA seasonal cycle at Dakar (**Fig 12a**) occurs outside of these burning season months and is therefore most likely due to changes in dust properties due to advection from differing dust source regions. There was relatively little seasonal variation for the three longer wavelengths, with an average annual SSA range <0.01 at 870 and 1020 nm. Note that the maximum SSA from the AERONET retrievals is ~0.993, due to a constraint on the minimum imaginary refractive index of 0.005 in all wavelengths. However, two other sites (Tamanrasset and Banizoumbou) showed lesser seasonal cycles at 440 nm and of a different annual shape. The Tamanrasset site SSA as a function of day of year is shown in **Figure 12b**. Very low SSA values for all wavelengths occurred sporadically from Day 110-200 at Tamanrasset, with lowest values at 440 nm ranging from ~0.85 to ~0.70. It is possible that dark and absorbing airborne sediments eroded from multiple sources, potentially including the volcano Waw an Namus in the Libyan Desert, may have contributed to these very low SSA values. Note that satellite images of the Waw an Namus volcanic site shows almost black volcanic rock plus a trade wind deposited plume of dark sediment that extends downwind ~100 km to the southwest from the core volcanic area.

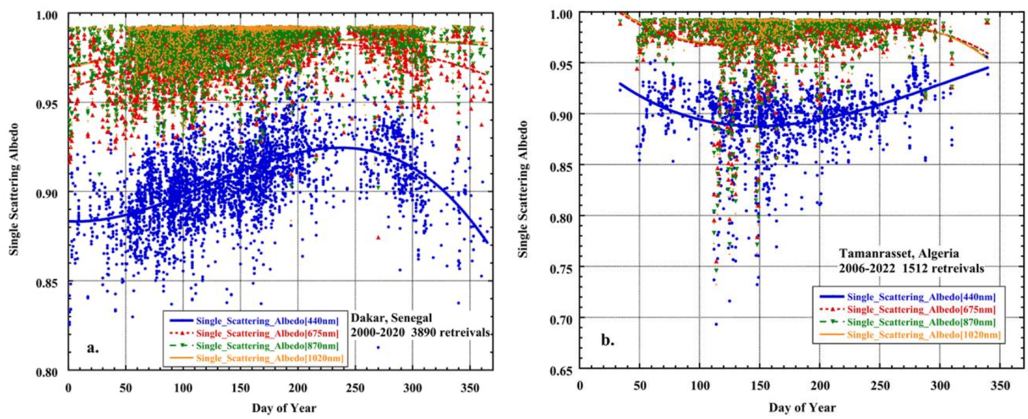


**Figure 12. Spectral SSA variation at 440, 675, 870 and 1020 nm as a function of day of the year for (a) the Dakar, Senegal site and (b) the Tamanrasset, Algeria site.**

A comparison of SSA on two dust dominated days for the Ilorin site in conjunction with HYSPLIT trajectory analyses (**Figure 13**) show that the measured SSA was significantly higher when the trajectory was over the Bodele versus the other day when the trajectory was from another region of the Sahara/Sahel. This is consistent with the known properties of the Bodele depression dust which is very weakly absorbing (white color and low iron oxide content of this diatomaceous sediment deposit; Hudson-Edwards et al., 2014; Di Biagio et al., 2019). Additionally, an experimental retrieval with the 380 nm and 500 nm wavelengths added showed very close agreement with the 3rd order spectral fit at the other 4 wavelengths. An extrapolation of the 3rd order polynomial fit to the V3 four-

https://doi.org/10.5194/egusphere-2026-5531
Preprint. Discussion started: 18 September 2026




wavelength retrieval to 380 nm for these cases resulted in 380 nm SSA within <0.007 of the 6-wavelength retrievals for these two cases. This suggests that 3[rd] order polynomial fits can be used to extrapolate the 4 wavelength retrievals to 380 nm thereby making accurate estimates of 380 nm SSA for dust case aerosols from older instrument data in the AERONET database. Additionally, this is also a robust way to interpolate to 500 nm SSA with V3 four-channel retrievals since the agreement is even better at that wavelength. Therefore the 3[rd] order polynomial fit would also be an accurate way to interpolate SSA to the commonly analyzed satellite retrieval and/or aerosol modeled mid-visible wavelengths of 520 to 550 nm (Li et al., 2024; Li et al., 2025).

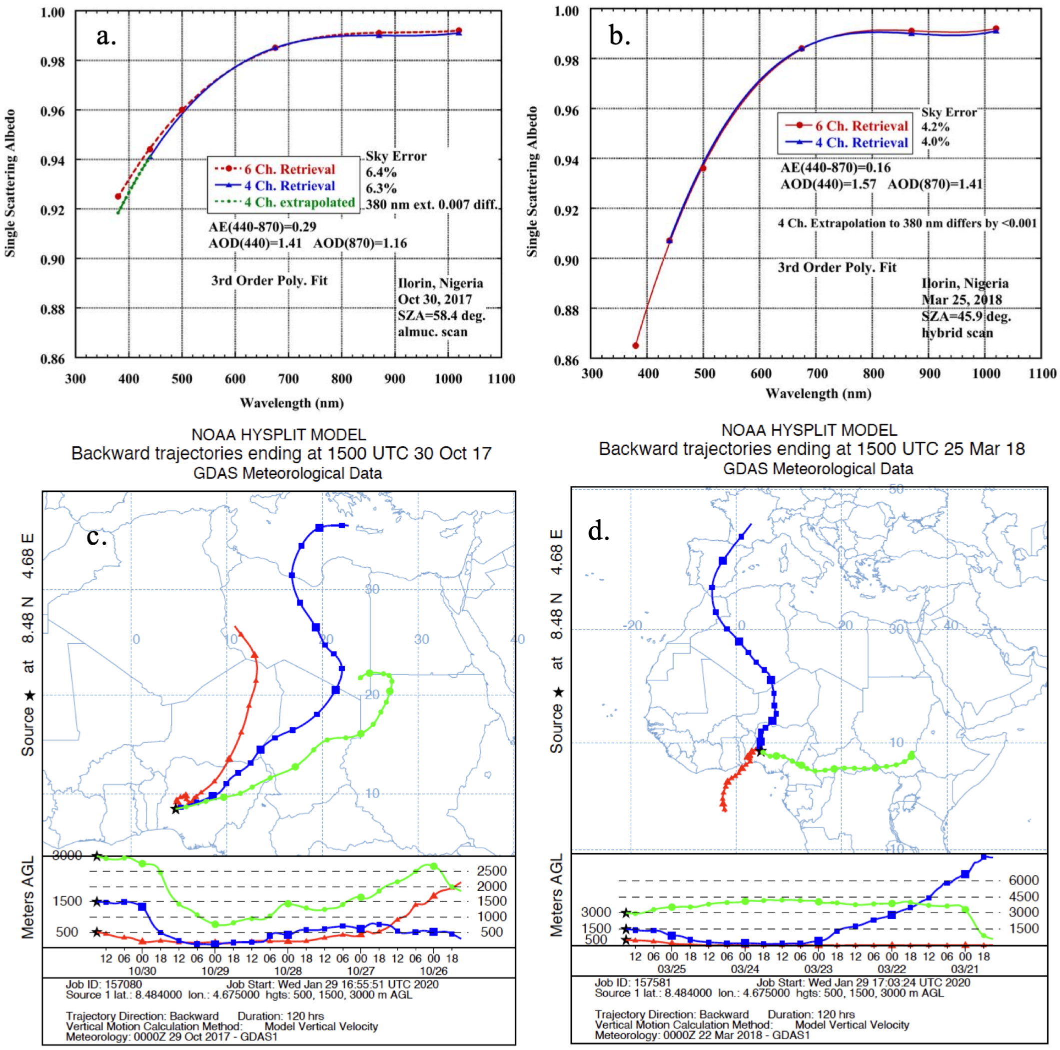


**Figure 13. Spectral variation of SSA at the Ilorin, Nigeria site for two selected L2 retrievals for dust cases (AE<0.3) on (a) October 30, 2017 at SZA=58.5 and (b) on March 25, 2018 at SZA=45.9. The standard 4-channnel inversion of V3 is compared to a preliminary experimental 6-channel inversion that adds the 380 and 500 nm wavelengths. Both dates and**

https://doi.org/10.5194/egusphere-2026-5531
Preprint. Discussion started: 18 September 2026




**channel inputs are fit with a 3rd order polynomial as a function of wavelength, showing that an extrapolation of SSA by the 4-channel fit to 380 nm results in very small differences (0.0007 and 0.001 respectively) as compared to the 6-channel retrievals at 380 nm. Back trajectories computed by the HYSPLIT model for (c) the Oct 30, 2017 SSA spectra case shown in (a) and (d) for the Mar 25, 2018 SSA spectra case shown in (b).**

### 3.2.2 Refractive Index

Comparisons of the AERONET multi-year database of retrievals of spectral imaginary refractive index to those estimated values from the study of DB19 are also analyzed. While the SSA of Di Biagio et al. (2019) are computed directly from scattering and absorption coefficient measurements, the imaginary refractive index is computed by them from Mie code using the measured size distributions and optical data. Since the dust was (erroneously) assumed by DB19 to be spherical this introduces some uncertainty in their calculated refractive indices (Kong et al., 2024). Therefore, the larger differences in this parameter versus the AERONET retrieved values at Dakar (**Figure 14**) may be in part ascribed to the greater uncertainty of the DB19 values as compared to their measurements of SSA. **Figure 15** shows the multi-year means of the AERONET retrieved imaginary part (a) and real part (b) of the refractive index (IRI and RRI respectively) for all 9 primary sites analyzed. For the imaginary part the values (also **Table 2**) show significant variation at 440 nm likely due to differences in iron oxide content while the longer wavelengths show similarly small values with reduced variability indicative of relatively weak absorption at all sites. The AERONET retrieval means of real refractive index (RRI) for the Sahel and Sahara sites were ~1.45 ±0.02 for all four wavelengths as compared to the DB19 computed values of 1.49 to 1.52 for the same region which are significantly higher. Kandler et al. (2009) also determined a higher RRI for dust in Morocco based on chemical and mineralogical composition, ranging from ~1.57 at 440 to ~1.54 at 1020 nm. It is noted however that the RRI retrieved by AERONET is the parameter with the lowest accuracy (Sinyuk et al. 2020). For the Australia, Gobi Desert and Saudi Arabian desert AERONET sites the average retrieved RRI values were nearly all >1.50, with the Australian site having the highest of 1.52-1.54 which is similar to the 1.54 calculated by DB19 from Australian soil samples. The AERONET retrieved RRI at the Solar Village site in Saudi Arabia ranged from ~1.50 to 1.53 which is also close to the 1.50-1.55 range computed by DB19 from soil samples in the Middle East and northeast Africa. The large geographical variations of real and complex refractive indices are indicative of large variations of dust mineralogy and consequently lidar ratio (Schuster et al., 2012; Nisantzi et al., 2015). The lidar ratio is a key variable for accurate retrievals of dust extinction from backscatter lidars.

https://doi.org/10.5194/egusphere-2026-5531
Preprint. Discussion started: 18 September 2026




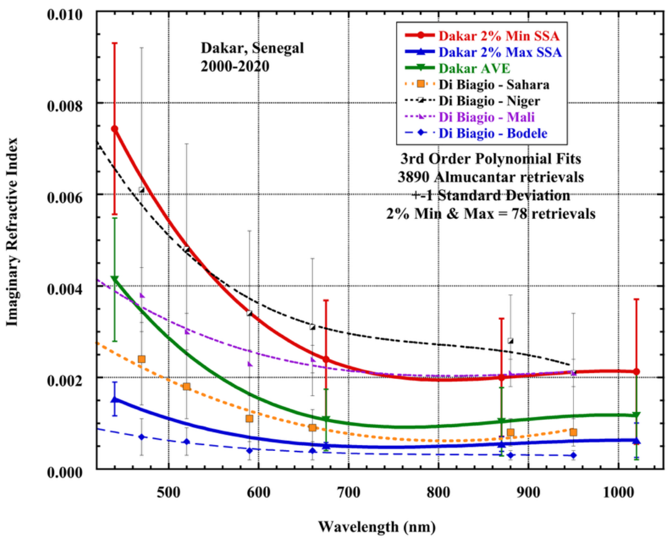


**Figure 14. Similar to Figure 7 for the Dakar, Senegal site dust cases but for the climatological data of the AERONET retrieved spectral imaginary refractive index versus computed values from the DB19 dust generated from soil samples in the Sahara and Sahel.**

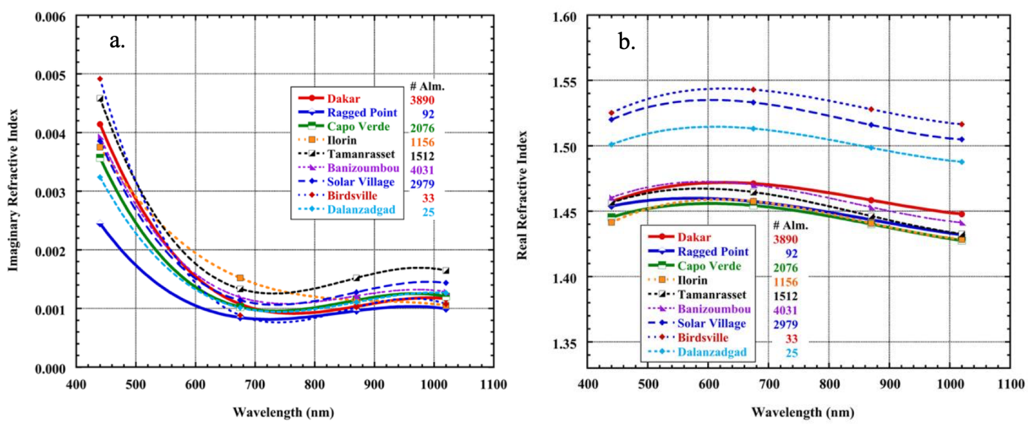


**Figure 15. Climatological averages of (a) spectral imaginary refractive index and (b) spectral real refractive index for nine sites with multi-year monitoring. Six sites have robust statistics with ~1100 to ~4000 almucantar retrievals averaged per site while the other three sites (Ragged Point, Birdsville and Dalanzadgad) have much smaller sample sizes due to AOD typically being much lower than the applied threshold of AOD(440)>0.4.**

https://doi.org/10.5194/egusphere-2026-5531
Preprint. Discussion started: 18 September 2026




**Table 2. Spectral imaginary refractive index (IRI) averages and standard deviations computed from multi-year monitoring at the nine primary sites for dust cases where AOD(440)>0.4 and AE<0.4. N is the number of almucantar scans.**

| Site | 440 nm IRI ave | 675 nm IRI ave | 870 nm IRI ave | 1020 nm IRI ave | 440 nm IRI std | 675 nm IRI std | 870 nm IRI std | 1020 nm IRI std | N |
|---|---|---|---|---|---|---|---|---|---|
| **Dakar** | 0.00414 | 0.00107 | 0.00103 | 0.00117 | 0.00135 | 0.00067 | 0.00074 | 0.00096 | 3890 |
| **Capo Verde** | 0.00357 | 0.00102 | 0.00114 | 0.00120 | 0.00145 | 0.00093 | 0.00113 | 0.00126 | 2076 |
| **Banizoumbou** | 0.00393 | 0.00119 | 0.00121 | 0.00128 | 0.00151 | 0.00097 | 0.00112 | 0.00136 | 4031 |
| **Tamanrasset** | 0.00458 | 0.00133 | 0.00152 | 0.00164 | 0.00281 | 0.00198 | 0.00249 | 0.00293 | 1512 |
| **Ilorin** | 0.00375 | 0.00152 | 0.00114 | 0.00105 | 0.00124 | 0.00083 | 0.00082 | 0.00088 | 1156 |
| **Solar Village** | 0.00385 | 0.00114 | 0.00128 | 0.00144 | 0.00130 | 0.00086 | 0.00112 | 0.00132 | 2979 |
| **Ragged Point** | 0.00245 | 0.00084 | 0.00096 | 0.00099 | 0.00078 | 0.00084 | 0.00106 | 0.00124 | 92 |
| **Birdsville** | 0.00491 | 0.00088 | 0.00102 | 0.00108 | 0.00176 | 0.00050 | 0.00057 | 0.00072 | 33 |
| **Dalanzadgad** | 0.00324 | 0.00101 | 0.00111 | 0.00126 | 0.00060 | 0.00053 | 0.00067 | 0.00088 | 25 |

### 3.2.3 Asymmetry Parameter

The asymmetry parameter is another important physical characteristic in assessing the direct radiative forcing of atmospheric aerosols (Zhao et al., 2018). The asymmetry parameter (g) which characterizes the anisotropy of light scattering in particles is also computed from the AERONET retrievals. It is calculated as the cosine-weighted average of the scattering phase function, with values defined as ranging from -1 (complete backscattering) to +1 (complete forward scattering). **Figure 16** shows the multi-year means of the AERONET retrieved asymmetry parameters for all of the dust dominated site observations analyzed in this study. The g values at 440 nm for aerosol originating from the Sahel and Sahara regions range from ~0.79 to ~0.81, while at the longer wavelengths for this region the values are lower at ~0.76 ±0.01. For the other three sites (Solar Village, Birdsville and Dalanzadgad) the g values are similar to the Sahel/Sahara values at 440 nm but somewhat lower for 675 nm through 1020 nm at ~0.73 to 0.74. These are all relatively high values of g, consistent with strong forward scattering by coarse mode dust particles. Otto et al. (2008) simulated spectral values of g utilizing measured size distributions and chemical composition of a Saharan dust plume from in situ aircraft data in Morocco. They computed g ranging from ~0.81 at 440 nm to ~0.75 at 1020 nm which are very similar to the AERONET retrieved values for Saharan dust, however they assumed a spherical shaped particle assumption. They showed a steeper increase in g for wavelengths shorter than 600 nm, also similar to AERONET. It is noted that AERONET utilized a spheroidal particle shape assumption to compute g, and Otto et al. (2009) found differences of about ±1% at 440 nm and ranging from ~1% higher to up to ~4% lower at 1020 nm between spherical and spheroidal shape computations of g which were dependent on differing aspect ratio of the spheroids. Measurements of g for Saharan dust with no modeling involved were made by Horvath et al. (2018). They utilized a polar nephelometer located at a mountain site in southern Spain measuring scattering angles from $5^0$ to $175^0$ for Saharan dust transport events in June of 2016. The values of g they measured at 532 nm were ~0.7 to 0.76 for the Saharan dust dominated events with low scattering Angstrom Exponent <0.5. From Figure 16 and linearly interpolating in wavelength to 532 nm the AERONET value of g is ~0.78 to ~0.795 for the multi-year averages at the Sahel and Sahara sites which is ~0.055 higher than the dust events measured by Horvath et al. (2018). This a reasonable agreement given the standard deviation of g at 440 nm from AERONET data for

https://doi.org/10.5194/egusphere-2026-5531
Preprint. Discussion started: 18 September 2026




Sahara and Sahel sites ranged from 0.016 to 0.022 compared to only a few dust events measured by Horvath et al. (2018), plus the spectral linear interpolation between AERONET 440 nm and 675 nm data is an estimate for the mid-visible.

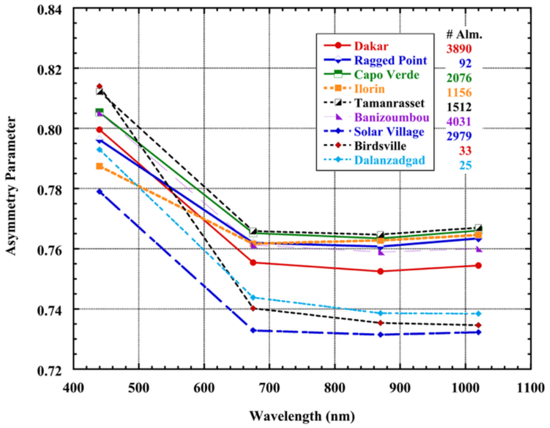


**Figure 16. Climatological averages of spectral asymmetry parameter for nine sites with multi-year monitoring. Six sites have robust statistics with ~1100 to ~4000 almucantar retrievals averaged per site while the other three sites (Ragged Point, Birdsville and Dalanzadgad) have much smaller sample sizes due to AOD typically being much lower than the applied threshold of AOD(440)>0.4.**

### 3.2.4 Volume Size Distributions

In this section we analyze the AERONET retrievals of aerosol volume size distributions concentrating on the retrievals obtained from multiyear data records which for some sites span an interval of two decades or longer. Additionally, we are focusing on the sub-micron or middle mode sized dust particles and not the coarse mode or super-micron sized dust. As mentioned previously, studies by Ryder et al. (2015) and Zheng et al. (2024) have shown that AERONET retrievals do not include sufficient large or giant mode dust particles in part due to low sensitivity to these large particles in the wavelength ranges of the V3 data AERONET retrievals and also due to an AERONET defined upper limit of the particle radius of 15 microns. Therefore in this section we emphasize the analysis of retrievals in the size range where the AERONET data have high sensitivity to particle size, the sub-micron radius range. Specifically AERONET has high sensitivity to fine mode particle size such as biomass burning particles (Reid et al., 2005) and urban/industrial aerosols (Schafer et al, 2019) and also to middle sized sub-micron aerosol such as aerosols of volcanic origin in the stratosphere (Boichu et al., 2023; Eck et al., 2010) and fog and cloud processed aerosols (Eck et al., 2012; Li et al., 2014).

https://doi.org/10.5194/egusphere-2026-5531
Preprint. Discussion started: 18 September 2026




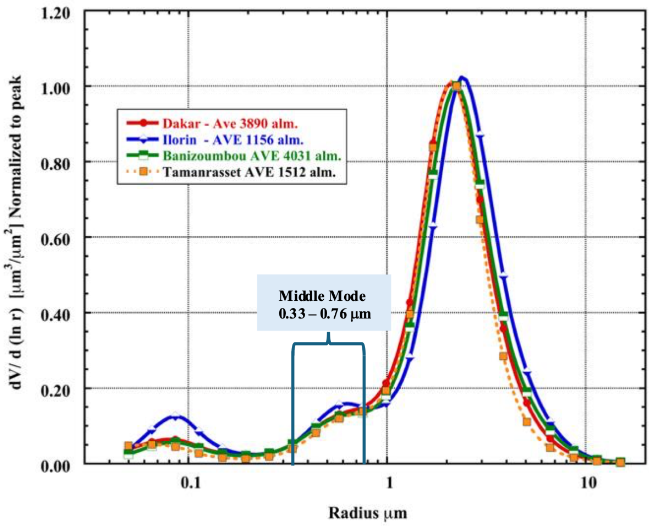


**Figure 17. Climatological averages of retrieved size distributions for four sites in the Sahel and Sahara region. All four sites show very similar middle (0.33-0.76 mm radius) and super-micron radius coarse modes.**

First we show a comparison of the multi-year averages of the retrieved volume size distributions for four sites in the Sahel and Sahara region in **Figure 17**. The sites are Dakar on the Atlantic coast of Senegal, Banizoumbou, Niger in the Sahel, Ilorin, Nigeria in the West Sudanian savanna zone, and Tamanrasset, Algeria in the central Saharan Desert. The data shown are averages normalized to the peak value computed from ~1100 to ~4000 individual almucantar retrievals for each of these sites. The 'middle mode' sized particles (volume radius from 0.33 to 0.76 µm) are present in site averages of AERONET retrievals for all four of these sites in the Sahara and Sahel, for dust cases when AOD(440)>0.4 and AE(440-870)<0.4. Since there is no local minimum between modes this middle mode was typically split between the AERONET computed fine and coarse modes where the average fine-coarse delimitator radius was ~0.444 to 0.459 µm for these four sites (close to the minimum value of 0.439 µm). This persistent middle mode results in a large fine mode fraction of aerosol optical depth (~40% at 440 nm; if fine mode is defined as radius<0.76 mm) for the majority of dust events from the world's largest sources of airborne soil dust. Additionally, this middle mode of diameters 0.66 to 1.52 mm is well within the $PM_{2.5}$ size range of aerodynamic diameter <2.5 micron, therefore readily inhalable and a significant human health risk (Yang et al., 2022). Middle mode sized dust particles were also observed from in situ aircraft sampling during the GERBILS campaign in the western Sahara and Sahel in June 2007 as reported by Johnson and Osborne (2011). These were averaged size distributions from flights that transited thousands of kilometers over this dust source region. These in situ campaign averaged size distributions agreed very well with AERONET retrievals made at two sites within the aircraft sampled spatial domain for the middle mode region (sub-micron radius). The AERONET size distributions were 12-day averages over the same time interval as the aircraft flights in late June 2007. For the coarse mode the in situ data showed slightly smaller radius peak coarse mode radius and also a relatively small tail of larger radius dust

https://doi.org/10.5194/egusphere-2026-5531
Preprint. Discussion started: 18 September 2026




that the AERONET retrievals did not detect, therefore consistent with AERONET underestimation of the largest dust particles.

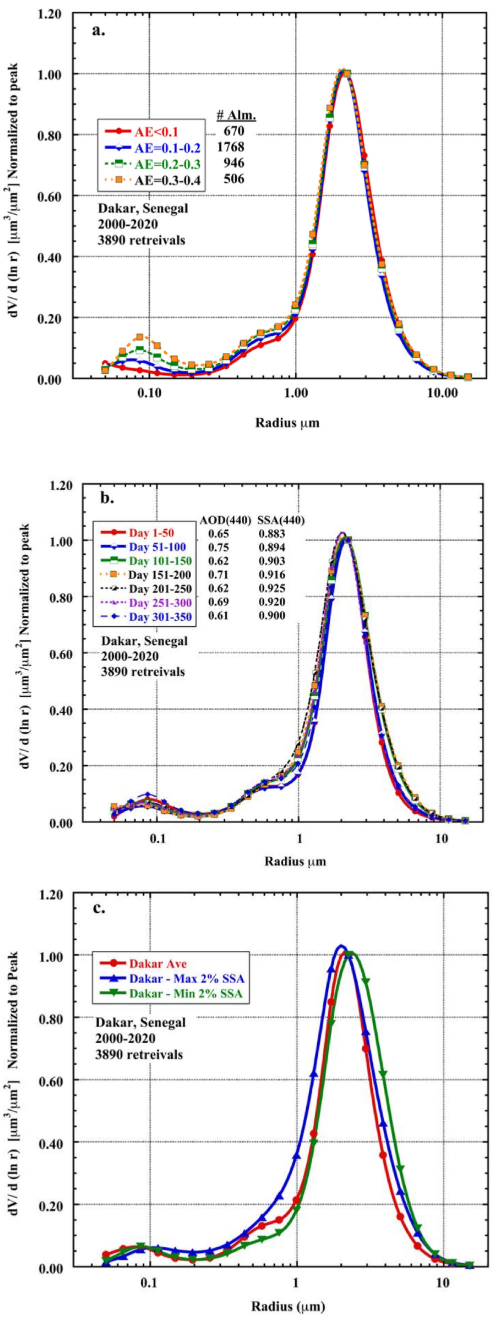


**Figure 18. Climatological averages of retrieved size distributions for the Dakar site as a function of (a) Angstrom Exponent (440-870 nm) in 0.1 bin averages and (b) day-of-year in 50-day bin averages. (c) Size distributions**

https://doi.org/10.5194/egusphere-2026-5531
Preprint. Discussion started: 18 September 2026




**corresponding to Figure 7 of SSA retrievals for the overall average of 3890 almucantar retrievals and for the 2% highest and lowest magnitude SSA retrievals.**

The sizes of AERONET retrieved middle mode and coarse particles are very similar to widely utilized sediment particle size classifications which designate clay particle radius range from ~0.02 µm to a maximum of 1 µm and silt particles from 1 µm to a maximum of ~25 to 31 µm radius (Blott and Pye, 2012), with sand particles being larger than the upper limit of silt sizes. Therefore, the middle mode in AERONET data is equivalent in size to clay particles while the coarse mode is equivalent to silt-sized particles. Clay minerals are typical components of Saharan/Sahelian airborne dust, for example Caquineau et al. (1998) measured clay minerals in dust transported to Cape Verde Island.

Next we show analyses of the variation in the average volume size distribution (normalized to peak) as a function of the magnitude of AE(440-870) in bins of 0.1 (**Figure 18a)** and also how it varies throughout the annual cycle at one site, Dakar, Senegal in **Figure 18b**. The coarse mode (radius >1 micron) was very similar for all ranges of Angstrom Exponent (440-870) < 0.4, showing insignificant variation. The middle mode (radius 0.33 – 0.76 mm) showed a small decrease for AE<0.1 while the other three AE ranges were similar (Fig 18a). Therefore, the middle mode was persistent and quite similar for all AE values. The fine mode (radius <0.33 µm) showed the largest variation as a function of AE range, which may be due to fine mode dust particles or fine mode combustion aerosols, likely a combination of these two types of aerosols. **Figure 18b** shows the average volume size distributions for the Dakar site throughout the annual cycle in 50-day interval bins. Note that the average AOD of each bin is similarly high ranging from 0.61 to 0.75 at 440 nm (minimum value set at 0.4 at 440 nm). Overall the size distributions showed very little relative variation throughout the annual cycle, with slighter wider coarse mode from day 101 through day 250. The middle mode (~0.33 – 0.76 µm radius) and fine size particles were present throughout the year in relatively similar relative concentrations. This relative stability of the fine mode (<0.33 µm) suggests that the AE <0.4 filter removed most smoke-dust mixture cases from the data analyzed at this site, and that much of this fine mode may possibly be dust particles. The presence of the middle mode throughout the annual cycle also suggests the possibility that this dust mode may be produced from multiple dust sources and not just from one or a few single dust source regions. AlNassar et al. (2024) analyzed the dust frequency and relative contributions of all major dust sources in the Sahel, Sahara and Middle East regions using geostationary satellite data. They concluded that the two most significant sources in terms of percentage source area contribution for this entire region were the Bodele Depression and the Talak Desert located in very distinct areas. The Bodele was found to be the dominant source in the 3-month interval of Dec-Feb while the Talak Desert was the dominant source in Jun-Aug. The relatively small annual variation in the retrieved size distributions shown in **Figure 18b** therefore suggests that these two distinct source regions may possibly produce quite similar particle size distributions. We also examine the average size distributions at Dakar associated with the highest and lowest 2% of SSA retrieved at 440 nm (**see Figure 7**) in comparison with the average of all retrievals in **Figure 18c**. The least absorbing 2% of SSA retrievals have a slightly larger middle mode plus a larger shoulder of submicron radius particles which together are the radius range of most efficient particle scattering. The most absorbing 2% of SSA retrievals have the opposite, a somewhat smaller middle

https://doi.org/10.5194/egusphere-2026-5531
Preprint. Discussion started: 18 September 2026




mode and slightly larger coarse mode thereby having somewhat less efficient particle scattering. Therefore, differences in size distribution contribute to the retrieved extremes in SSA through differences in scattering efficiency however the large differences in imaginary refractive index at the 2% extremes (**see Figure 14**) due to particle iron oxide content are the main drivers of SSA magnitude variability. It is noted that in situ measurements of mid and long range transported dust (Adebiyi et al., 2023; Formenti and DiBiagio, 2024) show the presence of fine and middle mode particles for dust observations. We plot the LEV2b data of Formenti and DiBiagio (2024) from global in situ dust measurements but with linear instead of logarithmic y-axis and also normalized to the peak value of the size distributions in **Figure 19**. Their data shows a dominance of submicron radius particles for long-range transported dust plumes and a significant submicron radius shoulder for mid-range transported dust.

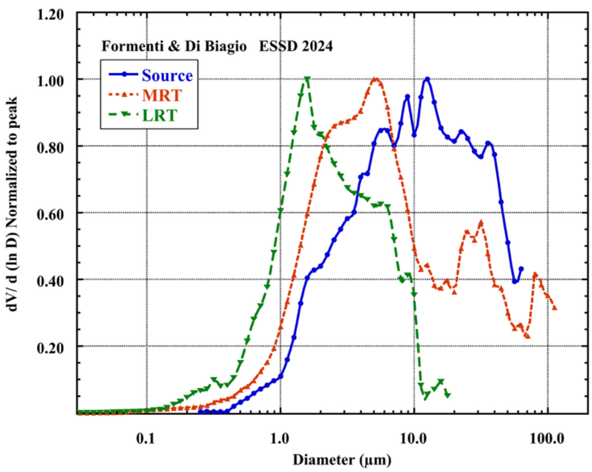


**Figure 19. Formenti and DiBiagio (2024) LEV2b aerosol size distribution data from global in situ dust measurements plotted with linear y-axis scale and also normalized to the peak value of the size distributions. Source refers to data acquired near to the dust source region, MRT is data acquired after medium range transport and LRT to data acquired after long-range transport.**

The multi-year average volume size distributions, normalized to the peak value, for the nine AERONET sites analyzed in depth in this study are shown in **Figure 20**. The super-micron radius coarse mode is similar for all sites except for Birdsville in Australia, the same site that is also the outlier for low SSA values. The sites in the Arabian Peninsula (Solar Village) and the Gobi Desert (Dalanzadgad) both showed very similar coarse mode peak radius and width to the Sahel, Sahara and Caribbean sites while the retrievals from Birdsville, Australia exhibited larger coarse mode radius with a wider modal distribution. However as previously mentioned the V3 AERONET retrievals have relatively limited sensitivity to the larger radius end of the coarse mode and very limited sensitivity to giant mode size particles. The sub-micron middle mode for Solar Village was similar to that for the Saharan site of Tamanrasset. The middle mode was less pronounced for the Australian and Gobi Desert site retrievals, however there is still a significant middle mode shoulder distribution for these sites as well suggesting that this size mode is present in dust from most source regions. The small fine mode (<0.33 mm radius) is quite similar for all sites except Ilorin, Nigeria site which is located in a city and therefore has a significant source of urban/industrial combustion aerosols.

https://doi.org/10.5194/egusphere-2026-5531
Preprint. Discussion started: 18 September 2026




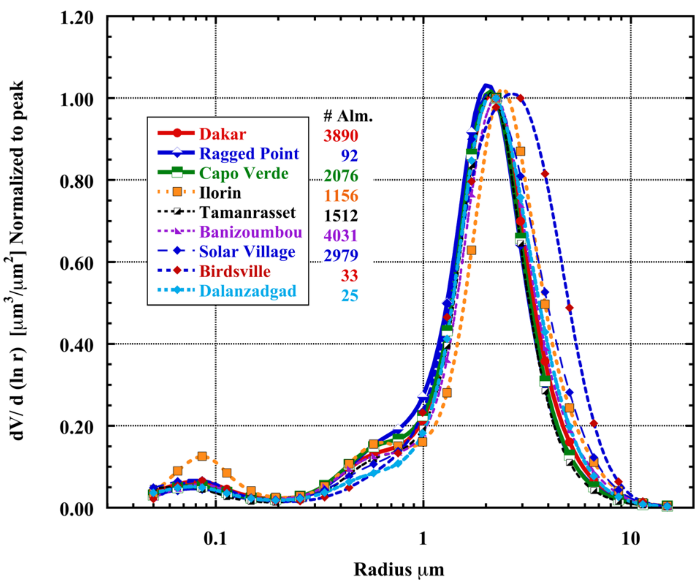


**Figure 20. Climatological averages of retrieved dust size distributions for nine sites with multi-year monitoring. Six sites have robust statistics with ~1100 to ~4000 almucantar retrievals averaged per site while the other three sites (Ragged Point, Birdsville and Dalanzadgad) have much smaller sample sizes due to AOD typically being much lower than the applied threshold of AOD(440)>0.4.**

AERONET provides both the complete size distribution retrievals at 22 radius values from 0.05 to 15 μm (shown in all previous analyses in this paper) and additionally lognormal fits of these volume size distributions for two modes, fine and coarse. These lognormal fits of the AERONET size distributions are often utilized by the satellite remote sensing community in their development of aerosol type models (Castellanos et al., 2024). An exception is the Multiangle Imaging SpectroRadiometer (MISR) instrument algorithm dust model which does include a prominent intermediate size mainly sub-micron radius mode (Kalashnikova et al. (2005); Kalashnikova and Kahn (2006)). Likewise, the OPAC model also includes this mode (Hess et al., 1998). A comparison of the two AERONET volume size distributions for the multi-year mean data from the Dakar site is shown in **Figure 21**. These average size distributions were computed from 3890 Level 2 retrievals over a 20-year interval. There are differences in both the super- and sub-micron distributions. Very similar differences are seen for dust size distributions at other sites (not shown). The lognormal fit has a broader coarse mode extending to smaller radii into the sub-micron size range, while the lognormal fine mode is intermediate between the two submicron modes. Notably the middle mode is significantly diminished in the lognormal fit that combines both the fine and coarse lognormal modes. Castellanos et al (2024) showed a similar comparison of an AERONET retrieved size distribution to the lognormal fits for a single very high AOD (2.79 at 440 nm) dust case (AE(440-870)=0.09) at the Capo Verde site. The AERONET retrieved complete size distribution for this case fit the AOD spectra to within 1.2% or less (~0.01 to 0.033 in AOD) at the 4 input wavelengths (440, 675, 870, 1020 nm). This retrieval had a significant middle mode, while the log-normal parameters also given in the AERONET retrieval diminished this middle mode. Computed spectral AOD

https://doi.org/10.5194/egusphere-2026-5531
Preprint. Discussion started: 18 September 2026




with the lognormal fit distribution did not exhibit the full magnitude of the measured spectral drop-off in AOD at 1020 nm, thus the lognormal fit of two modes did not reproduce the AOD spectra as well for this case. However, the computed spectral SSA was essentially same with either size distribution applied.

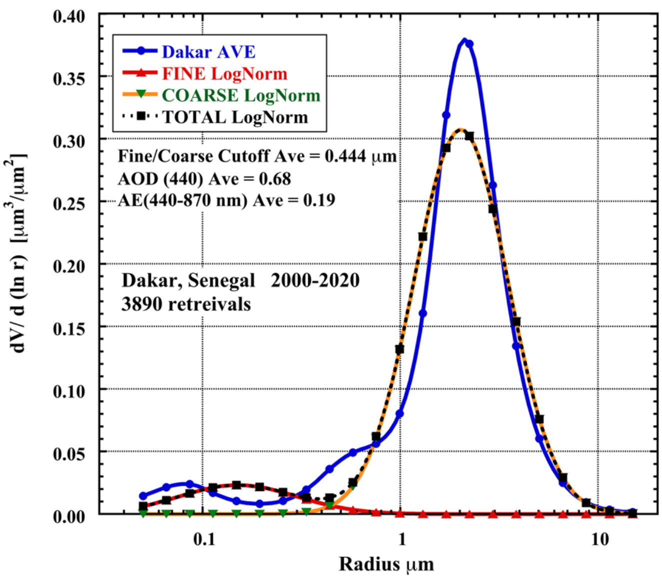


**Figure 21. AERONET retrieved climatological average size distribution at the Dakar site for all 22 radius values (blue solid line) versus the lognormal fits of the fine and coarse modes as defined by AERONET. Note that the sum of the fine and coarse mode lognormal distributions (black dashed line) results in a much reduced middle-sized mode and a broader coarse mode.**

### 3.2.5 Spectral AOD

A comparison of example dust cases to examine the sensitivity of the UV to shortwave infrared AOD spectra to changes in the size distribution is given in **Figure 22**. Both of these selected Level 2 retrievals at the Birdsville and Dakar sites have very low AE(440-870) of less than 0.08 yet the Dakar case has a significantly smaller radius coarse mode plus a distinct shoulder that encompasses a significant middle sized particle radius range. The Birdsville case size distribution has minimal sub-micron particles and is unusual for dust cases since the vast majority have significant middle mode sized particles. The AOD spectra at Birdsville is linear in logarithmic space (Angstrom fit) also unusual for a dust case, with all 8 wavelengths from 340 to 1640 nm fit to within less than 0.006 in AOD. In contrast the Dakar case shows a relatively large decrease in AOD at 1640 nm which is consistent with the presence of significant middle mode sub-micron sized particles and which is typical in AOD spectra for observations of most dust dominated aerosol. A linear fit to 6 wavelengths (380 to 1020 nm) for this Dakar case is within 0.01 for all 6 channels yet when extrapolated to 1640 nm it is ~0.11 too high. Therefore, the lack of a middle

https://doi.org/10.5194/egusphere-2026-5531
Preprint. Discussion started: 18 September 2026




mode plus larger size coarse mode particles in the Birdsville case likely contributed to the lack of significant spectral drop-off at 1640 nm while the presence of middle mode sized particles in the Dakar case likely contributed to the relatively large decrease in AOD at 1640 nm. Both cases exhibited typical SSA spectra for dust with significantly lower values at 440 nm relative to 675 nm, with SSA differences (675 nm - 440 nm) of 0.145 for the Birdsville case and 0.071 for the Dakar case. The SSA at 440 nm was 0.794 for the Birdsville case and 0.92 for the Dakar case. The retrievals in both cases were made with 100% spheroidal particle shape consistent with dust aerosol non-sphericity. For the Birdsville case the real refractive index was 1.530 to 1.551 increasing with wavelength from 440 to 1020 nm while for the Dakar case it varied from 1.443 to 1.416, decreasing with wavelength from 440 to 1020 nm. Therefore, the magnitude and spectral variation of the real refractive index of these cases may also have been a factor in the spectral variation of AOD especially at 1640 nm (see following discussion and Figure 23b).

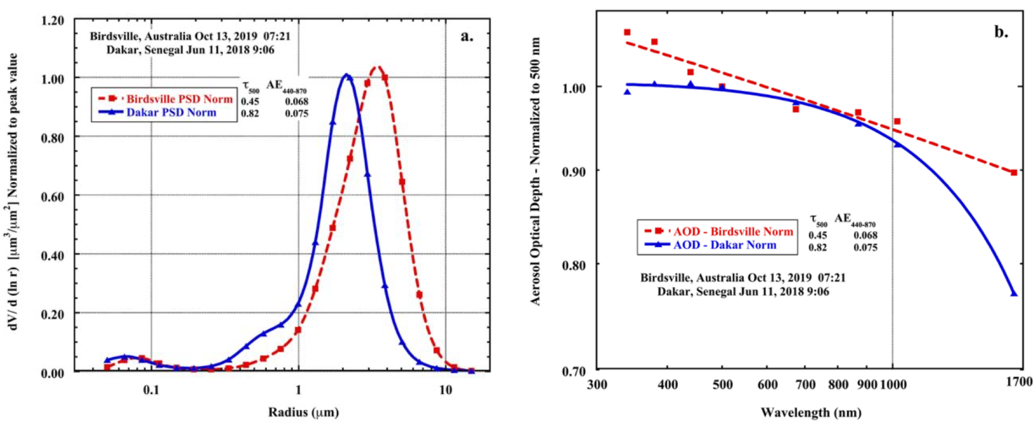


**Figure 22. Comparison of selected dust cases of retrieved size distributions (a) and measured direct sun AOD spectra (b) at two sites: Birdsville, Australia on Oct 13, 2019 and Dakar, Senegal on Jun 11, 2018. Both were L2 almucantar retrievals with very low and similar AE(440-870) of ~0.07.**

In order to investigate the influence of the middle mode dust size distribution, particle shape and real refractive index on the spectral variation of AOD from 440 to 1640 nm we made calculations utilizing the multi-year averaged size distribution and complex refractive index retrievals from the 4-channel V3 inversions at the Tamanrasset site (see Figures 15 and 17). The imaginary refractive index at 1640 nm was assumed to be equal to the value at 1020 nm and the real refractive index at 1640 nm was estimated to be 1.37 by extrapolation from a linear fit to the 675 to 1020 nm values. For simulation purposes we minimized the middle mode and fine mode of this volume size distribution to a modified size distribution (**Figure 23a**) in order to compute the AOD spectra both with and without significant middle mode influence. Additionally, we computed the AOD spectra for the multi-year averaged size distribution and refractive indices for both the spheroidal particle shape and the spherical shape assumptions. From **Figure 23b** we see that the spheroidal particle shape assumption results in lower AOD at 1640 nm than the spherical shape assumption, as was similarly shown by Hansell et al. (2011). Additionally, **Figure 23b** shows that a wavelength independent value of real refractive index of 1.456 (the multi-year average value at 440 nm) resulted in

https://doi.org/10.5194/egusphere-2026-5531
Preprint. Discussion started: 18 September 2026




higher AOD at 1640 nm as compared to a real refractive index of 1.37 at 1640 nm. However, the removal of the middle mode sized particles had a much larger effect on the AOD spectra, resulting in a significant increase in AOD at 1640 nm relative to 1020 nm (**Figure 23b)**. We note that such an increase in AOD from 1020 nm to 1640 nm has never been observed in AERONET measured spectra for dust dominated aerosol cases. This same type of spectral increase at ~1640 nm relative to ~870 nm AOD was found in computations by Castellanos et al. (2024) for the assumed size distributions and refractive indices utilized in some satellite retrieval algorithms. For example, in the MAIAC retrieval algorithm there is a minimal middle mode in the assumed size distribution plus high value of the real part of refractive index which was assumed spectrally flat at 1.56. For spheroidal particle shape and these MAIAC assumed dust properties Castellanos et al. (2024) computed an AOD spectra that showed an increase from ~870 nm to ~1640 nm.

We also examined an experimental AERONET retrieval where the spectral AOD and directional sky radiance data from 500 nm and 1640 nm were added to the standard four channels (440, 675, 870, 1020 nm). This six channel inversion of an almucantar scan from the Tamanrasset site on April 11, 2024 fits the direct sun measured AOD to all wavelengths to within ~0.01, which is typical for AERONET retrievals. The retrieved value of the real refractive index at 1640 nm was 1.39 for this case. The size distribution from this experimental 6-channel retrieval is compared to the standard 4-channel retrieval in **Figure 23c**. Two clear differences in these retrieved size distributions are the significantly larger volume of the middle mode and the significantly larger radius of the coarse mode in the 6-channel retrieval. Therefore, in order to fit the measured AOD at 1640 nm an even larger middle mode was required, thereby further suggesting that middle mode particles are a significant fraction of dust AOD.

We additionally analyze the multi-year average characteristics of the AOD spectra measurements at selected sites and cases dominated by Saharan/Sahelian dust aerosol. First, AOD spectra data ranging from 380 nm to 1640 nm from the Tamanrasset site in Algeria located in the mid-Sahara are shown in **Figure 24a**. These are all Level 2 AOD data from 2015-2022 for the criteria of AOD>0.4 and Angstrom 440-870 <0.4, to be consistent with the dust retrieval data parameter thresholds in previous sections. There were a total of 8357 instantaneous AOD spectra utilized here with averages computed as a function of AOD at 440 nm in bins of 0.2 width, except for the highest AOD bin which is much wider to encompass the long tail of highest values. Most of the measurements were in the lowest 3 AOD bins therefore <1.0 at 440 nm. Only AOD spectra that had all wavelengths from 380 to 1640 nm were utilized here, with the 340 nm excluded since that is the wavelength that most often did not meet the L2 quality control criteria especially in the earlier years of the data record. Note that the average AE for all bins is quite low ranging from the highest value of 0.13 for the lowest AOD bin, decreasing to 0.03 for the highest AOD bin. The average AOD data in each bin at all wavelengths were normalized to AOD at 500 nm. Second order polynomials (in linear coordinates – not the standard logarithmic) fit the averaged AOD spectra very well from 380 to 1640 nm, within the AERONET AOD measurement uncertainty of 0.01-0.02 (higher in the UV) for the entire range of AOD. Note the significant decrease in AOD at 1640 nm relative to 870 and 1020 nm, especially for the higher AOD bins that had lowest AE. This is due in part to the middle mode sized particles (~0.33-0.76 mm radius; **Figure 17**) which have a relatively small Angstrom Exponent (AE) in the visible to 870 nm but larger AE at longer wavelengths.

https://doi.org/10.5194/egusphere-2026-5531
Preprint. Discussion started: 18 September 2026




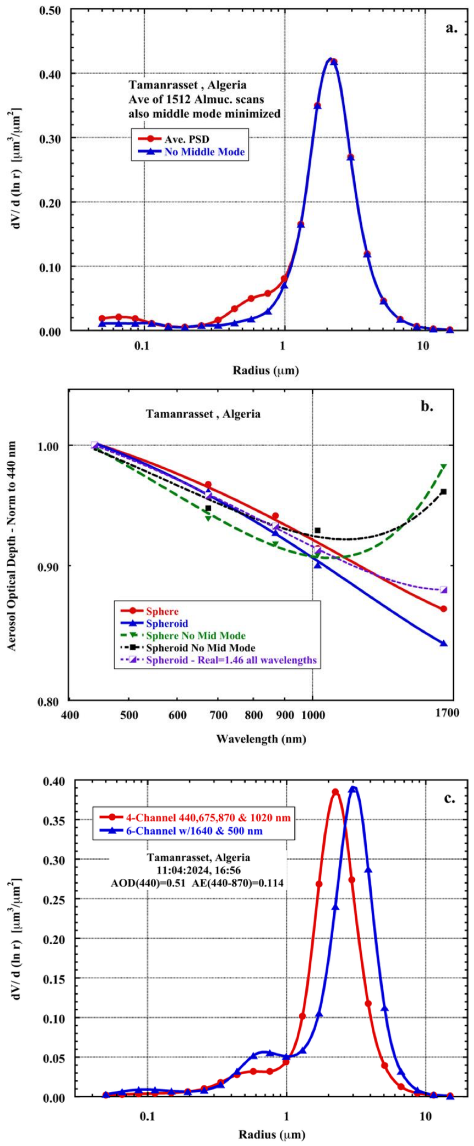


**Figure 23. (a) The average particle size distribution for the Tamanrasset site computed from all 1512 Level 2 V3 inversions (Red; see Figure 17) and this size distribution modified to minimize the sub-micron radius portion of the distribution (Blue). (b) Calculation of the spectral AOD from 440 nm to 1640 nm for the assumed particle shapes of both spherical and spheroidal using the unmodified average PSD, for the modified size distributions shown in (a) for both shape assumptions and for two different values of the Real part of the refractive index (see text for details). (c) The standard V3 4-channel retrieval of particle size distribution utilizing AOD and directional sky radiances at 440, 675, 870 and 1020 nm (in red) for a single almucantar scan dust case at the Tamanrasset site (April 11, 2024, 16:56 UTC). An**

https://doi.org/10.5194/egusphere-2026-5531
Preprint. Discussion started: 18 September 2026




**experimental retrieval (in blue) that includes the 500 nm and 1640 nm wavelengths in addition to the standard 4 wavelengths used in V3.**

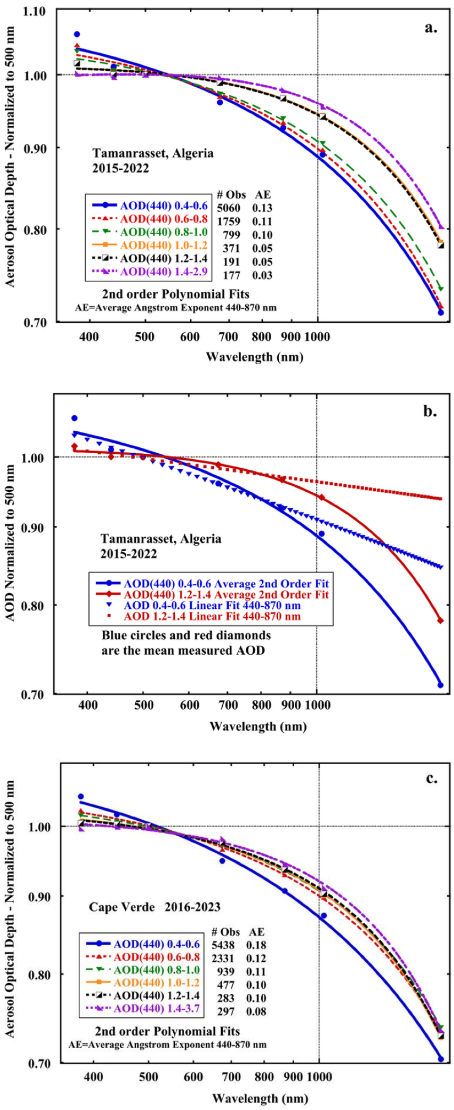


**Figure 24. (a) Direct sun measured L2 AOD spectra normalized to 500 nm from the Tamanrasset site for AOD(440)>0.4 and AE(440-870)<0.4. All AOD spectra have all seven measured wavelengths from 380 nm to 1640 nm, with data averaged in bins of 0.2 in 440 nm AOD, except for the highest AOD range bin. (b) The data for AOD(440) bins of 0.4-0.6 and 1.2-1.4 from (a) but also fitted with the linear (Angstrom) fit from 440 to 870 nm. (c) Similar to (a) but for measured AOD spectra normalized to 500 nm from the Cape Verde site.**

https://doi.org/10.5194/egusphere-2026-5531
Preprint. Discussion started: 18 September 2026




**Figure 24b** shows how a linear or Angstrom fit from 440 to 870 nm (using all 4 wavelengths in that interval) to estimate the AOD at 1640 nm would result in significant overestimates. For the spectra associated with AOD(440) averaged from 0.4 to 0.6 the linear Angstrom fit overestimated the AOD at 1640 by 0.07 (estimated 0.42 versus actual of 0.35), while for the average AOD(440) bin of 1.2-1.4 the Angstrom fit would overestimate the AOD at 1640 nm by 0.21 (estimated 1.22 versus actual of 1.01). Therefore, it is obvious that using the Angstrom linear fit from wavelengths shorter than 1020 nm in logarithmic coordinates would yield a very biased extrapolation estimate of AOD at 1640 nm.

Similar to **Figure 24a**, the averaged AOD spectra for the L2 data at the Cape Verde site from 2016-2023 are shown in **Figure 24c**. There were a total of 9765 instantaneous AOD spectra averaged into the AOD bins with average AE ranging somewhat higher at this site as compared to Tamanrasset, from AE of 0.18 for the lowest AOD bin to 0.08 at the highest AOD bin. Again, there is a notable decrease in AOD at the longest wavelengths, especially the large drop from 1020 nm to 1640 nm, likely due in large part to the persistently significant middle-mode in the volume size distribution for this site (**Figure 20**). Castellanos at al. (2024) computed the spectral AOD from the UV to >2000 nm for a variety of satellite remote sensing algorithm dust aerosol models. They showed a wide range of spectral variation of AOD in the longer wavelengths with some models showing little to no decrease from ~870 nm to ~1640 nm, or even an increase in AOD. This is consistent with some of these dust aerosol models having assumed size distributions with little to no middle mode sized aerosols. However, one of the Dark Target retrieval dust models investigated by Castellanos at al. (2024) exhibited a size distribution with a significant shoulder in the middle mode and also had very low real refractive index at all wavelengths (~1.37 to ~1.34). Their computed AOD spectra for this model showed similar significant decreases in AOD at ~1640 nm as AERONET measurements thereby consistent with our analysis of the influence of the middle mode and real part of refractive index on shortwave infrared AOD.

## 4. Summary and Conclusions

This paper examines AERONET retrieval products and AOD spectra for dust dominated observations in the world's major dust source regions therefore provides previously overlooked information that may be applicable to future studies that utilize the AERONET database.  Statistically robust AERONET data from multi-year monitoring were analyzed for airborne dust dominated observations with AE(440-870)<0.4 in five sites located in and immediately downwind of the world's largest dust source region of the Sahara and Sahel, plus one site in a part of the second largest dust source region, the Arabian Peninsula. Three additional sites with much smaller sample sizes due to significantly lower dust AOD were also studied. Observations with moderate to high AOD were analyzed (AOD(440)>0.4) in order to have high sensitivity to retrieved aerosol absorption parameters. This study focused on retrievals of the spectral dust absorption as parameterized by the SSA at four wavelengths from 440 to 1020 nm, the size distribution of dust cases with emphasis on the sub-micron radius sized particles, and the spectral measurements of AOD ranging from 380 to 1640 nm. The coarse mode (super-micron radius) dust size distributions were not emphasized since the spectral range of the AERONET optical measurements (440 to 1020 nm) utilized to retrieve

https://doi.org/10.5194/egusphere-2026-5531
Preprint. Discussion started: 18 September 2026




size distributions provides limited ability to detect giant sized dust particles in the range of 10 micron radius and larger.

The major findings of this study are as follows:

1) The AERONET retrievals of spectral SSA agreed very well with measured averages of dust generated in the lab from soil samples taken in the same regions from the study of DB19, which is the only other global source region measurement database of spectral SSA for dust. SSA differences for multi-year averaged retrievals at five AERONET sites in the Sahara and Sahel regions versus the DB19 spectral values for the Sahara averaged from 5 different soil sample locations in the region agreed to within <0.01 for the AERONET retrieval wavelengths of 440 nm through 1020 nm. SSA differences between the AERONET site in Saudi Arabia and the single DB19 soil sample from the Arabian Peninsula agreed to within 0.02 or less at all wavelengths. For the Gobi Desert AERONET site the averaged retrievals also showed excellent agreement with the Gobi soil sample from DB19, with SSA differences of less than 0.01 at all wavelengths.

2) Extremes of SSA defined from the two standard deviation tails defined as the highest and lowest 2% of all 440 nm SSA retrieved values of the AERONET multi-year retrieval database also agreed well with the most and least absorbing soil samples of DB19. For example, at the Dakar site the highest 2% of retrieved SSA values agreed with the least absorbing soil sample in the region (Bodele) within less than 0.015 and the agreement with the most absorbing soil samples in the Sahel region (Mali and Niger) was within ~0.03 or less. The AERONET retrievals of 440 nm SSA at each site were very close to normally distributed, therefore the 2% extremes are representative of two standard deviation tails.

3) The average SSA across most sites examined (except Australia and the Caribbean) converge to a similar value of ~0.91 ±0.01 at 440 nm, and ~0.98 at near infrared wavelengths. Thus, this is a reasonable baseline estimate for these major global sources of dust. However, this does not mean SSA is static; there are important spatial/temporal variabilities. Significant seasonal variation of SSA for dust dominated events was detected at some sites in the Sahel/Saharan region. At three sites (Ilorin, Dakar and Cape Verde) the 440 nm SSA showed similar seasonal cycles (although much smaller in amplitude at Cape Verde), with the SSA maxima occurring in July-August while the minima were in December-January. At Dakar the annual range in average SSA was ~0.04 at 440 nm with a minimum of ~0.885 and maximum of 0.925. In contrast there was little seasonal variability for the three longer wavelengths, with an average annual SSA range <0.01 at 870 and 1020 nm. However, at other sites (Tamanrasset and Banizoumbou) in the Sahara and Sahel a different seasonal cycle of SSA at 440 nm was observed. Such variation can result in significant seasonal spread in calculated absorption optical depth at some locations. Additionally, significant day-to-day variations can occur due to advection from different dust source regions that have different soil minerology. The lowest average SSA of all sites examined was in Australia, which is consistent with the lowest dust SSA from soil samples by DB19. The highest SSA of all sites was trans-Atlantic transported dust from the Sahara/Sahel to AERONET retrievals of SSA and measurements of spectral AOD have been widely utilized in several recently published works on the properties, distribution and effects or impacts of desert dust particles optical and physical properties. Barbados in the Caribbean possibly due in part to mixing with sea salt and hygroscopicity effects in the marine boundary layer.

https://doi.org/10.5194/egusphere-2026-5531
Preprint. Discussion started: 18 September 2026




4) The spectral variation of AERONET retrieved SSA from 380 to 1020 nm for dust cases can be fit well with a third order polynomial to within <0.01 (typically < 0.005) at all wavelengths. This has been shown with some experimental retrievals that include both 380 nm and 500 nm in addition to the standard four wavelengths from 440 nm to 1020 nm. Additionally spectral SSA variation of the soil sample lab measurements of BD19 are also accurately fit with a third order polynomial to within <0.01 (typically < 0.005) for the wavelength range of 370 to 950 nm. This is therefore a rigorous way to extrapolate the existing AERONET database of dust retrievals to SSA at 380 nm and to spectrally interpolate to the frequently utilized wavelength of 550 nm for satellite retrievals or aerosol model intercomparisons.

5) All sites in the Sahara and Sahel region and the one site in the Saudi Arabian Peninsula showed a significant sub-micron radius middle mode in the multi-year averaged volume size distributions. This mode was present throughout the year and at all levels of AE from less than 0.1 to 0.4 therefore a consistently present mode in the dust size distributions. This sub-micron mode is consistent with in situ measured dust size distributions that show similar or even larger contributions of these sub-micron radius particles from ~0.33 to 0.76 micron radius to the overall size distributions. AERONET retrievals suggest this mode constitutes a significant fraction (~40%) of the total AOD at 500 nm and is therefore important in remote sensing applications. The middle mode was also present in a site in the Gobi Desert of Mongolia and in a desert site in Australia but at a lesser magnitude than from the Saharan/Sahelian/Arabian sites. The middle mode is equivalent in size to clay sedimentary particles while the super-micron radius or coarse mode is consistent with silt sized particles. The smaller sub-micron dust particle size mode is more readily inhalable than the coarse mode and/or giant mode particles and therefore likely to be more harmful to human health.

6) An additional volume size distribution product from AERONET is the bi-modal log-normal fit consisting of a fine and coarse mode volume median radii plus the width of each mode. These log-normal fits result in significant size distribution differences as compared to the full 22 radius bin retrieved distributions, however they are often utilized to define particle size parameters for satellite remote sensing retrievals. One of the main differences is that the log-normal fit minimizes the sub-micron middle mode which is prevalent in the full-size distribution retrievals for dust. This minimization of the middle mode is not consistent with the significant spectral decrease in AOD at 1640 nm for most AERONET dust observation spectra.

7) Multi-year averages of AOD spectra from 380 to 1640 nm for sites in the Sahara and Sahel showed a persistent and significant decrease in AOD from 1020 nm to 1640 nm which can be explained at least in part by the presence of middle mode sized particles. Extrapolation of dust AOD spectra to 1640 nm from an Angstrom or linear fit in lognormal coordinates for wavelengths from 440 to 870 nm resulted in significant overestimation of measured AOD at 1640 nm. Simulations of AOD spectra from 440 to 1640 nm suggest that the largest influence on 1640 nm AOD for dust cases is the presence or absence of the middle mode size particles with the middle mode resulting in significantly lower AOD at 1640 nm. However, simulations showed that particle shape and real refractive index also influenced the AOD at 1640 nm with both spheroidal (versus spherical) shape and lower real refractive index resulting in lower AOD at 1640 nm.

https://doi.org/10.5194/egusphere-2026-5531
Preprint. Discussion started: 18 September 2026




AERONET retrievals of spectral SSA and measurements of spectral AOD have been widely utilized in several recently published works on the properties, distribution and effects or impacts of desert dust particles optical and physical properties. Overall, the findings presented here provide a more complete understanding of the AERONET retrieved SSA and it's spatial and temporal dynamics. Spectral SSA is a significant aerosol parameter that often has considerable uncertainty therefore the information presented here may help in improving assessments of the radiative and climatic impacts of desert dust. Although several previous works had identified the presence of a volume size distribution middle mode or sub-micron radius dust mode the current work suggests that this mode is essentially ubiquitous in the world's major dust source region of the Sahara/Sahel. Additionally, the multi-year characterization of average spectral AOD for Sahara/Sahel region dust aerosols from the UV to 1640 nm had not been fully documented previously and this also has implications for dust radiative effects across the solar spectrum.

Regarding the retrieved size distributions of dust aerosol from AERONET, it is recognized that the current particle shape assumption of spheroidal particles is an approximation that fits the data reasonably well however there are uncertainties associated with exact dust particle shapes. Therefore, future work may focus on AERONET retrievals with more physically robust particle shape assumptions and also with extended wavelength retrievals including the 1640 nm data thereby providing more sensitivity to dust size distributions, in particular for the coarse mode.

**Acknowledgements.** The AERONET project at NASA Goddard Space Flight Center (GSFC) is generously supported by the Atmosphere program within Earth System Science Research Program of NASA's Earth Science Division, as well as numerous field campaigns. We gratefully acknowledge the resources provided by the NASA High-End Computing (HEC) Program through the NASA Center for Climate Simulation (NCCS) at GSFC, which enabled the research and analysis presented here. We also wish to express our sincere appreciation to all Principal Investigators and site managers at AERONET stations worldwide for their continued commitment to building and maintaining ground-based observation networks. Finally, we are deeply grateful to the many AERONET partner networks, calibration centers, and funding agencies whose ongoing support sustains the AERONET program and advances atmospheric science globally.

**Data availability.** The data utilized in this study are available from the NASA Goddard Space Flight Center AERONET project webpage, https://aeronet.gsfc.nasa.gov .

https://doi.org/10.5194/egusphere-2026-5531
Preprint. Discussion started: 18 September 2026




## References


Adebiyi, A., Kok, J.F., Murray, B.J., Ryder, C.L., Stuut, J.B.W., Kahn, R.A., Knippertz, P., Formenti, P., Mahowald, N.M., García-Pando, C.P. and Klose, M., 2023. A review of coarse mineral dust in the Earth system. *Aeolian Research*, *60*, p.100849. DOI:10.1016/j.aeolia.2022.100849

Alfaro, S. C., S. Lafon, J. L. Rajot, P. Formenti, A. Gaudichet, and M. Maille´ (2004), Iron oxides and light absorption by pure desert dust: An experimental study, J. Geophys. Res., 109, D08208, doi:10.1029/2003JD004374. 1. Introduction

Alfaro-Contreras, R., Zhang, J., Reid, J. S., and Christopher, S.: A study of 15-year aerosol optical thickness and direct shortwave aerosol radiative effect trends using MODIS, MISR, CALIOP and CERES, Atmos. Chem. Phys., 17, 13849–13868, https://doi.org/10.5194/acp-17-13849-2017, 2017.

AlNasser, F., Chehbouni, A. and Entekhabi, D., 2024. Dust source areas and their plume extent derived from satellite data fields. *Geophysical Research Letters*, *51*(16), p.e2024GL110753 , doi: 10.1029/2024gl110753

Barreto, Á., Cuevas, E., Granados-Muñoz, M.-J., Alados-Arboledas, L., Romero, P. M., Gröbner, J., Kouremeti, N., Almansa, A. F., Stone, T., Toledano, C., Román, R., Sorokin, M., Holben, B., Canini, M., and Yela, M.: The new sun-sky-lunar Cimel CE318-T multiband photometer – a comprehensive performance evaluation, Atmos. Meas. Tech., 9, 631–654, https://doi.org/10.5194/amt-9-631-2016, 2016.

Blott, S.J. and Pye, K., 2012. Particle size scales and classification of sediment types based on particle size distributions: Review and recommended procedures. *Sedimentology*, *59*(7), pp.2071-2096. https://doi.org/10.1111/j.1365-3091.2012.01335.x

Bishop, J. K., Davis, R. E., & Sherman, J. T. (2002). Robotic observations of dust storm enhancement of carbon biomass in the North Pacific. *Science*, *298*(5594), 817-821, DOI: 10.1126/science.1074961

Boichu, M., Grandin, R., Blarel, L., Torres, B., Derimian, Y., Goloub, P., et al. (2023). Growth and global persistence of stratospheric sulfate aerosols from the 2022 Hunga Tonga–Hunga Ha'apai volcanic eruption. *Journal of Geophysical Research: Atmospheres*, 128, e2023JD039010. https://doi.org/10.1029/2023JD039010

Caquineau, S., Gaudichet, A., Gomes, L., Magonthier, M.C. and Chatenet, B., 1998. Saharan dust: Clay ratio as a relevant tracer to assess the origin of soil-derived aerosols. *Geophysical research letters*, *25*(7), pp.983-986. https://doi.org/10.1029/98GL00569

Carlson, T. N., and S. G. Benjamin, 1980: Radiative Heating Rates for Saharan Dust. *J. Atmos. Sci.*, **37**, 193–213, doi:10.1175/1520-0469(1980)037<0193:RHRFSD>2.0.CO;2

Cattrall, C., K. L. Carder, and H. R. Gordon (2003), Columnar aerosol single-scattering albedo and phase function retrieved from sky radiance over the ocean: Measurements of Saharan dust, *J. Geophys. Res.*, 108, 4287, doi:10.1029/2002JD002497, D9.

https://doi.org/10.5194/egusphere-2026-5531
Preprint. Discussion started: 18 September 2026




Castellanos, P., Colarco, P., Espinosa, W.R., Guzewich, S.D., Levy, R.C., Miller, R.L., Chin, M., Kahn, R.A., Kemppinen, O., Moosmüller, H. and Nowottnick, E.P., 2024. Mineral dust optical properties for remote sensing and global modeling: A review. *Remote Sensing of Environment*, *303*, p.113982.doi: 10.1016/j.rse.2023.113982

Clarke, A.D., Howell, S., Quinn, P.K., Bates, T.S., Ogren, J.A., Andrews, E., Jefferson, A., Massling, A., Mayol-Bracero, O., Maring, H. and Savoie, D., 2002. INDOEX aerosol: A comparison and summary of chemical, microphysical, and optical properties observed from land, ship, and aircraft. *Journal of Geophysical Research: Atmospheres*, *107*(D19), pp.INX2-32, doi:10.1029/2001JD000572

Di Biagio, C., Formenti, P., Balkanski, Y., Caponi, L., Cazaunau, M., Pangui, E., Journet, E., Nowak, S., Andreae, M. O., Kandler, K., Saeed, T., Piketh, S., Seibert, D., Williams, E., and Doussin, J.-F.: Complex refractive indices and single-scattering albedo of global dust aerosols in the shortwave spectrum and relationship to size and iron content, Atmos. Chem. Phys., 19, 15503–15531, https://doi.org/10.5194/acp-19-15503-2019, 2019.

Drake, N.A., Candy, I., Breeze, P., Armitage, S.J., Gasmi, N., Schwenninger, J.L., Peat, D. and Manning, K., 2022. Sedimentary and geomorphic evidence of Saharan megalakes: A synthesis. *Quaternary Science Reviews*, *276*, p.107318, doi: 10.1016/j.quascirev.2021.107318.

Dubovik, O., King, M.D., 2000. A flexible inversion algorithm for the retrieval of aerosol optical properties from Sun and sky radiance measurements. J. Geophys. Res. 105, 20,673– 20,696. DOI: 10.1029/2000JD900282

Dubovik, O., Holben, B., Eck, T.F., Smirnov, A., Kaufman, Y.J., King, M.D., Tanré, D. and Slutsker, I., 2002. Variability of absorption and optical properties of key aerosol types observed in worldwide locations. *Journal of the atmospheric sciences*, *59*(3), pp.590-608. DOI:https://doi.org/10.1175/1520-0469(2002)059<0590:VOAAOP>2.0.CO;2

Dubovik, O., Sinyuk, A., Lapyonok, T., Holben, B.N., Mishchenko, M., Yang, P., Eck, T.F., Volten, H., Mu~noz, O., Veihelmann, B., van der Zande, W.J., Leon, J.-F., Sorokin, M., Slutsker, I., 2006. The application of spheroid models to account for aerosol particle nonsphericity in remote sensing of desert dust. J. Geophys. Res. 111, D11208. https://doi.org/10.1029/2005JD006619.

Dubovik, O., Smirnov, A., Holben, B.N., King, M.D., Kaufman, Y.J., Eck, T.F., Slutsker, I., 2000. Accuracy assessments of aerosol optical properties retrieved from AERONET Sun and sky-radiance measurements. J. Geophys. Res. 105, 9791–9806.https://doi.org/10.1029/2000JD900040

Eck, T.F., Holben, B.N., Reid, J.S., Dubovik, O., Smirnov, A., O'Neill, N.T., Slutsker, I., Kinne, S., 1999. Wavelength dependence of the optical depth of biomass burning, urban, and desert dust aerosols. J. Geophys. Res. 104 (D24), 31,333–31,349. https://doi.org/10.1029/1999JD900923

Eck, T.F., Holben, B.N., Sinyuk, A., Pinker, R.T., Goloub, P., Chen, H., Chatenet, B., Li, Z., Singh, R.P., Tripathi, S.N., Reid, J.S., Giles, D.M., Dubovik, O., O'Neill, N.T., Smirnov, A., Wang, P., Xia, X., 2010. Climatological aspects of the optical properties of fine/coarse mode aerosol mixtures. J. Geophys. Res. 115, D19205. https://doi. org/10.1029/2010JD014002.

https://doi.org/10.5194/egusphere-2026-5531
Preprint. Discussion started: 18 September 2026




Eck, T.F., Holben, B.N., Reid, J.S., Giles, D.M., Rivas, M.A., et al., 2012. Fog- and cloud induced aerosol modification observed by the Aerosol Robotic Network (AERONET). J. Geophys. Res. Atmos.. http://dx.doi.org/10.1029/2011jd016839.

Eck, T.F., Holben, B.N., Giles, D.M., Slutsker, I., Sinyuk, A., Schafer, J.S., Smirnov, A., Sorokin, M., Reid, J.S., Sayer, A.M. and Hsu, N.C., 2019. AERONET remotely sensed measurements and retrievals of biomass burning aerosol optical properties during the 2015 Indonesian burning season. *Journal of Geophysical Research: Atmospheres*, *124*(8), pp.4722-4740. https://doi.org/10.1029/2018JD030182

Engelbrecht, J. P., Moosmüller, H., Pincock, S., Jayanty, R. K. M., Lersch, T., and Casuccio, G.: Technical note: Mineralogical, chemical, morphological, and optical interrelationships of mineral dust re-suspensions, Atmos. Chem. Phys., 16, 10809–10830, https://doi.org/10.5194/acp-16-10809-2016, 2016.

Evan, A. T., Flamant, C., Gaetani, M., & Guichard, F. (2016). The past, present and future of African dust. Nature, 531(7595), 493-495. doi: 10.1038/nature17149

Fiedler, S., K. Schepanski, B. Heinold, P. Knippertz, and I. Tegen (2013), Climatology of nocturnal low-level jets over North Africa and implications for modeling mineral dust emission, *J. Geophys. Res. Atmos.*, 118, 6100–6121, doi:10.1002/jgrd.50394.

Formenti, P., Schütz, L., Balkanski, Y., Desboeufs, K., Ebert, M., Kandler, K., Petzold, A., Scheuvens, D., Weinbruch, S., and Zhang, D.: Recent progress in understanding physical and chemical properties of African and Asian mineral dust, Atmos. Chem. Phys., 11, 8231–8256, https://doi.org/10.5194/acp-11-8231-2011, 2011.

Formenti, P., & Di Biagio, C. (2024). Large synthesis of in situ field measurements of the size distribution of mineral dust aerosols across their life cycles. *Earth System Science Data*, *16*(11), 4995-5007, https://doi.org/10.5194/essd-16-4995-2024, 2024.

Gavrouzou, M., Hatzianastassiou, N., Gkikas, A., Korras-Carraca, M.-B., Mihalopoulos, N. A., (2021) Global Climatology of Dust Aerosols Based on Satellite Data: Spatial, Seasonal and Inter-Annual Patterns over the Period 2005–2019. *Remote Sensing*; 13(3):359. https://doi.org/10.3390/rs13030359

Gianelli, S.M., Lacis, A.A., Carlson, B.E. and Hameed, S., 2013. Evidence of a weakly absorbing intermediate mode of aerosols in AERONET data from Saharan and Sahelian sites. *Journal of Geophysical Research: Atmospheres*, *118*(22), 12-661. https://doi.org/10.1002/2013JD020342

Giles, D. M., Sinyuk, A., Sorokin, M. G., Schafer, J. S., Smirnov, A., Slutsker, I., et al. (2019). Advancements in the Aerosol Robotic Network (AERONET) Version 3 database—Automated near-real-time quality control algorithm with improved cloud screening for Sun photometer aerosol optical depth (AOD) measurements. Atmospheric Measurement Techniques, 12, 169-209. https://doi.org/10.5194/amt-12-169-2019

Ginoux, P., Chin, M., Tegen, I., Prospero, J.M., Holben, B., Dubovik, O. and Lin, S.J., 2001. Sources and distributions of dust aerosols simulated with the GOCART model. *Journal of Geophysical Research: Atmospheres*, *106*(D17), pp.20255-20273. https://doi.org/10.1029/2000JD000053

Go, S., Lyapustin, A., Schuster, G. L., Choi, M., Ginoux, P., Chin, M., Kalashnikova, O., Dubovik, O., Kim, J., da Silva, A., Holben, B., and Reid, J. S.: Inferring iron-oxide species content in atmospheric mineral dust from

https://doi.org/10.5194/egusphere-2026-5531
Preprint. Discussion started: 18 September 2026




DSCOVR EPIC observations, Atmos. Chem. Phys., 22, 1395–1423, https://doi.org/10.5194/acp-22-1395-2022, 2022.

Go, S., Lyapustin A, Choi M, Korkin S, Wang Y and Hyer EJ (2025) MAIAC-based climatology of atmospheric iron-oxide dust species from DSCOVR EPIC observations. Front. Remote Sens. 6:1676851. doi: 10.3389/frsen.2025.1676851

Gomes, L., G. Bergametti, G. Coudé-Gaussen, and P. Rognon (1990), Submicron desert dusts: A sandblasting process, *J. Geophys. Res.*, 95(D9), 13927–13935, doi:10.1029/JD095iD09p13927.

Gonçalves Ageitos, M., Obiso, V., Miller, R. L., Jorba, O., Klose, M., Dawson, M., Balkanski, Y., Perlwitz, J., Basart, S., Di Tomaso, E., Escribano, J., Macchia, F., Montané, G., Mahowald, N. M., Green, R. O., Thompson, D. R., and Pérez García-Pando, C.: Modeling dust mineralogical composition: sensitivity to soil mineralogy atlases and their expected climate impacts, Atmos. Chem. Phys., 23, 8623–8657, https://doi.org/10.5194/acp-23-8623-2023, 2023.

Goudie, A.S., 2014. Desert dust and human health disorders. *Environment international*, *63*, pp.101-113.doi: 10.1016/j.envint.2013.10.011

Guirado, C., Cuevas, E., Cachorro, V. E., Toledano, C., Alonso-Pérez, S., Bustos, J. J., Basart, S., Romero, P. M., Camino, C., Mimouni, M., Zeudmi, L., Goloub, P., Baldasano, J. M., and de Frutos, A. M.: Aerosol characterization at the Saharan AERONET site Tamanrasset, Atmos. Chem. Phys., 14, 11753–11773, https://doi.org/10.5194/acp-14-11753-2014, 2014.

Hansell Jr., R. A., Reid, J. S., Tsay, S. C., Roush, T. L., and Kalashnikova, O. V.: A sensitivity study on the effects of particle chemistry, asphericity and size on the mass extinction efficiency of mineral dust in the earth's atmosphere: from the near to thermal IR, Atmos. Chem. Phys., 11, 1527–1547, https://doi.org/10.5194/acp-11-1527-2011, 2011.

Herman, J. R., P. K. Bhartia, O. Torres, C. Hsu, C. Seftor, and E. Celarier (1997), Global distribution of UV-absorbing aerosols from Nimbus 7/TOMS data, *J. Geophys. Res.*, 102(D14), 16911–16922, doi:10.1029/96JD03680.

Hess, M., P. Koepke, and I. Schult, 1998: Optical Properties of Aerosols and Clouds: The Software Package OPAC. *Bull. Amer. Meteor. Soc.*, **79**, 831–844, https://doi.org/10.1175/1520-0477(1998)079<0831:OPOAAC>2.0.CO;2.

Holben, B. N., Eck, T. F., Slutsker, I., Tanre, D., Buis, J. P., Setzer, A., et al. (1998). AERONET—A federated instrument network and data archive for aerosol characterization. Remote Sensing of Environment, 66(1), 1–16. doi: 10.1016/S0034-4257(98)00031-5

Holben, B. N., et al. (2001), An emerging ground-based aerosol climatology: Aerosol optical depth from AERONET, *J. Geophys. Res.*, 106(D11), 12067–12097, doi:10.1029/2001JD900014.

Holben, B. N., Eck, T. F., Slutsker, I., Smirnov, A., Sinyuk, A., Schafer, J., et al. (2006). AERONET's version 2.0 quality assurance criteria. Remote Sensing of Atmosphere and Clouds, Proceedings of SPIE - The International Society for Optical Engineering, 6408, 64080Q. https://doi.org/10.1117/12.706524

https://doi.org/10.5194/egusphere-2026-5531
Preprint. Discussion started: 18 September 2026




Horvath, H., Alados Arboledas, L., and Olmo Reyes, F. J.: Angular scattering of the Sahara dust aerosol, Atmos. Chem. Phys., 18, 17735–17744, https://doi.org/10.5194/acp-18-17735-2018, 2018.

Hudson-Edwards, K.A., Bristow, C.S., Cibin, G., Mason, G. and Peacock, C.L., 2014. Solid-phase phosphorus speciation in Saharan Bodélé Depression dusts and source sediments. *Chemical Geology*, *384*, pp.16-26., 10.1016/j.chemgeo.2014.06.014.

Husar, R. B., et al. (2001), Asian dust events of April 1998, *J. Geophys. Res.*, 106(D16), 18317–18330, doi:10.1029/2000JD900788.

Johnson, B. T., S. R. Osborne, J. M. Haywood, and M. A. J. Harrison (2008), Aircraft measurements of biomass burning aerosol over West Africa during DABEX, J. Geophys. Res., 113, D00C06, doi:10.1029/2007JD009451.

Johnson, B. T., S. Christopher, J. M. Haywood, S. R. Osborne, S. McFarlane, C. Hsu, C. Salustrod, and R. Kahn (2009), Measurements of aerosol properties from aircraft, satellite and ground-based remote sensing: A case-study from the Dust and Biomass-burning Experiment (DABEX), Q. J. R. Meteorol. Soc., 135, 922–934, https://doi.org/10.1002/qj.420

Johnson, B. T. and Osborne, S. R. (2011). Physical and optical properties of mineral dust aerosol measured by aircraft during the GERBILS campaign. Quarterly Journal of the Royal Meteorological Society, 137(658), 1117–1130. https://doi.org/10.1002/qj.777

Kalashnikova, O. V., R. Kahn, I. N. Sokolik, and W.-H. Li (2005), Ability of multiangle remote sensing observations to identify and distinguish mineral dust types: Optical models and retrievals of optically thick plumes, *J. Geophys. Res.*, 110, D18S14, doi:10.1029/2004JD004550.

Kalashnikova, O.V., Kahn, R., 2006. Ability of multiangle remote sensing observations to identify and distinguish mineral dust types: 2. Sensitivity over dark water. J Geophys Res Atmospheres. https://doi.org/10.1029/2005jd006756, 1984 2012 111.

Kandler, K., Schütz, L., Deutscher, C., Ebert, M., Hofmann, H., Jäckel, S., Jaenicke, R., Knippertz, P., Lieke, K., Massling, A. and Petzold, A., 2009. Size distribution, mass concentration, chemical and mineralogical composition and derived optical parameters of the boundary layer aerosol at Tinfou, Morocco, during SAMUM 2006. *Tellus B: Chemical and Physical Meteorology*, *61*(1), pp.32-50. https://doi.org/10.1111/j.1600-0889.2008.00385.x

Kim, D., Chin, M., Schuster, G., Yu, H., Takemura, T., Tuccella, P., et al. (2024). Where dust comes from: Global assessment of dust source attributions with AeroCom models. Journal of Geophysical Research: Atmospheres, 129, e2024JD041377. https://doi.org/10.1029/2024JD041377

Kim, D., Chin, M., Yu, H., Eck, T. F., Sinyuk, A., Smirnov, A., and Holben, B. N.: Dust optical properties over North Africa and Arabian Peninsula derived from the AERONET dataset, Atmos. Chem. Phys., 11, 10733–10741, https://doi.org/10.5194/acp-11-10733-2011, 2011.

Kok, J.F., Ridley, D.A., Zhou, Q., Miller, R.L., Zhao, C., Heald, C.L., Ward, D.S., Albani, S. and Haustein, K., 2017. Smaller desert dust cooling effect estimated from analysis of dust size and abundance. *Nature Geoscience*, *10*(4), pp.274-278. doi:10.1038/ngeo2912

https://doi.org/10.5194/egusphere-2026-5531
Preprint. Discussion started: 18 September 2026




Kok, J. F., Adebiyi, A. A., Albani, S., Balkanski, Y., Checa-Garcia, R., Chin, M., Colarco, P. R., Hamilton, D. S., Huang, Y., Ito, A., Klose, M., Li, L., Mahowald, N. M., Miller, R. L., Obiso, V., Pérez García-Pando, C., Rocha-Lima, A., and Wan, J. S.: Contribution of the world's main dust source regions to the global cycle of desert dust, Atmos. Chem. Phys., 21, 8169–8193, https://doi.org/10.5194/acp-21-8169-2021, 2021.

Kong, S., Wang, Z., and Bi, L.: Uncertainties in laboratory-measured shortwave refractive indices of mineral dust aerosols and derived optical properties: a theoretical assessment, Atmos. Chem. Phys., 24, 6911–6935, https://doi.org/10.5194/acp-24-6911-2024, 2024.

Leahy, L. V., Anderson, T. L., Eck, T. F., & Bergstrom, R. W. (2007). A synthesis of single scattering albedo of biomass burning aerosol over southern Africa during SAFARI 2000. Geophysical Research Letters, 34, L12814. https://doi.org/10.1029/2007GL029697

Leung, D. M., Kok, J. F., Li, L., Lawrence, D. M., Mahowald, N. M., Tilmes, S., and Kluzek, E.: A global dust emission dataset for estimating dust radiative forcings in climate models, Atmos. Chem. Phys., 25, 2311–2331, https://doi.org/10.5194/acp-25-2311-2025, 2025.

Li, D., Zhang, Y., Saito, M., Yang, P., & Hu, Y. (2025). The impact of dust mineralogical compositions on CALIOP-IIR-based retrievals of the optical and microphysical properties of dust plumes. Journal of Geophysical Research: Atmospheres, 130, e2025JD043829. https://doi.org/10.1029/2025JD043829

Li, L., Mahowald, N. M., Miller, R. L., Pérez García-Pando, C., Klose, M., Hamilton, D. S., Gonçalves Ageitos, M., Ginoux, P., Balkanski, Y., Green, R. O., Kalashnikova, O., Kok, J. F., Obiso, V., Paynter, D., and Thompson, D. R.: Quantifying the range of the dust direct radiative effect due to source mineralogy uncertainty, Atmos. Chem. Phys., 21, 3973–4005, https://doi.org/10.5194/acp-21-3973-2021, 2021.

Li, L., Mahowald, N.M., Gonçalves Ageitos, M., Obiso, V., Miller, R.L., Pérez García-Pando, C., Di Biagio, C., Formenti, P., Brodrick, P.G., Clark, R.N. and Green, R.O., 2024. Improved constraints on hematite refractive index for estimating climatic effects of dust aerosols. *Communications Earth & Environment*, *5*(1), p.295. doi:10.1038/s43247-024-01441-4.

Li, L., Mahowald, N. M., Obiso, V., Kok, J. F., Miller, R. L., Liu, X., et al. (2025). Dust direct radiative effect including large particles and component minerals. Geophysical Research Letters, 52, e2025GL119383. https://doi.org/10.1029/2025GL119383

Li, X., Mauzerall, D.L. & Bergin, M.H. Global reduction of solar power generation efficiency due to aerosols and panel soiling. *Nat Sustain* **3**, 720–727 (2020). https://doi.org/10.1038/s41893-020-0553-2

Li, Z., Eck, T., Zhang, Y., Zhang, Y., Li, D., Li, L., Xu, H., Hou, W., Lv, Y., Goloub, P. and Gu, X., 2014. Observations of residual submicron fine aerosol particles related to cloud and fog processing during a major pollution event in Beijing. *Atmospheric Environment*, *86*, pp.187-192. doi:10.1016/j.atmosenv.2013.12.044

Lwin, K.S., Tobias, A., Chua, P.L., Yuan, L., Thawonmas, R., Ith, S., Htay, Z.W., Yu, L.S., Yamasaki, L., Roqué, M. and Querol, X., 2023. Effects of desert dust and sandstorms on human health: a scoping review. *Geohealth*, *7*(3), p.e2022GH000728. DOI: 10.1029/2022GH000728

https://doi.org/10.5194/egusphere-2026-5531
Preprint. Discussion started: 18 September 2026




Lyapustin, A., Go, S., Korkin, S., Wang, Y., Torres, O., Jethva, H. and Marshak, A.: Retrievals of Aerosol Optical Depth and Spectral Absorption from DSCOVR EPIC. Front. Remote Sens., 2, 645794, https://doi.org/10.3389/frsen.2021.645794, 2021.

Malm, W. C., B. A. Schichtel, M. L. Pitchford, L. L. Ashbaugh, and R. A. Eldred (2004), Spatial and monthly trends in speciated fine particle concentration in the United States, *J. Geophys. Res.*, 109, D03306, doi:10.1029/2003JD003739.

Maring, H., D. L. Savoie, M. A. Izaguirre, L. Custals, and J. S. Reid (2003), Mineral dust aerosol size distribution change during atmospheric transport, *J. Geophys. Res.*, 108, 8592, doi:10.1029/2002JD002536, D19.

Marusak, L. A., Messier, R., & White, W. B. (1980). Optical absorption spectrum of hematite, α $Fe_2O_3$ near IR to UV. *Journal of Physics and Chemistry of Solids*, 41(9), 981-984, DOI:10.1016/0022-3697(80)90105-5

Mayol-Bracero, O.L., Prospero, J.M., Sarangi, B., Andrews, E., Colarco, P.R., Cuevas, E., Di Girolamo, L., Garcia, R.D., Gaston, C., Holben, B. and Ladino, L.A., 2025. "Godzilla", the extreme African dust event of June 2020: Origins, Transport, and Impact on Air Quality in the Greater Caribbean Basin. *Bulletin of the American Meteorological Society*, pp.BAMS-D. https://doi.org/10.1175/BAMS-D-24-0045.1

Mitchell, R. M., Forgan, B. W., and Campbell, S. K.: The Climatology of Australian Aerosol, Atmos. Chem. Phys., 17, 5131–5154, https://doi.org/10.5194/acp-17-5131-2017, 2017.

N'Datchoh, E. T., Konaré, A., Diedhiou, A., Diawara, A., Quansah, E., and Assamoi, P.: Effects of climate variability on savannah fire regimes in West Africa, Earth Syst. Dynam., 6, 161–174, https://doi.org/10.5194/esd-6-161-2015, 2015.

Nisantzi, A., Mamouri, R. E., Ansmann, A., Schuster, G. L., and Hadjimitsis, D. G.: Middle East versus Saharan dust extinction-to-backscatter ratios, Atmos. Chem. Phys., 15, 7071–7084, https://doi.org/10.5194/acp-15-7071-2015, 2015.

Obiso, V., Gonçalves Ageitos, M., Pérez García-Pando, C., Perlwitz, J. P., Schuster, G. L., Bauer, S. E., Di Biagio, C., Formenti, P., Tsigaridis, K., and Miller, R. L.: Observationally constrained regional variations of shortwave absorption by iron oxides emphasize the cooling effect of dust, Atmos. Chem. Phys., 24, 5337–5367, https://doi.org/10.5194/acp-24-5337-2024, 2024.

O'Neill, N. T., T. F. Eck, B. N. Holben, A. Smirnov, O. Dubovik, and A. Royer (2001), Bimodal size distribution influences on the variation of Angstrom derivatives in spectral and optical depth space, *J. Geophys. Res.*, 106(D9), 9787–9806, doi:10.1029/2000JD900245.

O'Neill, N.T., Eck, T.F., Smirnov, A., Holben, B.N. and Thulasiraman, S., 2003. Spectral discrimination of coarse and fine mode optical depth. *Journal of Geophysical Research: Atmospheres*, *108*(D17). https://doi.org/10.1029/2002JD002975

O'Neill, N. T., Ranjbar, K., Ivănescu, L., Eck, T. F., Reid, J. S., Giles, D. M., Pérez-Ramírez, D., and Chaubey, J. P.: Relationship between the sub-micron fraction (SMF) and fine-mode fraction (FMF) in the context of AERONET retrievals, Atmos. Meas. Tech., 16, 1103–1120, https://doi.org/10.5194/amt-16-1103-2023, 2023.

Otto, S., de Reus, M., Trautmann, T., Thomas, A., Wendisch, M., and Borrmann, S.: Atmospheric radiative effects of an in situ measured Saharan dust plume and the role of large particles, Atmos. Chem. Phys., 7, 4887–4903, https://doi.org/10.5194/acp-7-4887-2007, 2007.

Otto, S., E. Bierwirth, B. Weinzierl, K. Kandler, M. Esselborn, M. Tesche, A. Schladitz, M. Wendisch and T. Trautmann (2009) Solar radiative effects of a Saharan dust plume observed during SAMUM assuming spheroidal model particles, Tellus B: Chemical and Physical Meteorology, 61:1, 270-296, DOI: 10.1111/j.1600-0889.2008.00389.x

Panta, A., Kandler, K., Alastuey, A., González-Flórez, C., González-Romero, A., Klose, M., Querol, X., Reche, C., Yus-Díez, J., and Pérez García-Pando, C.: Insights into the single-particle composition, size, mixing state, and aspect ratio of freshly emitted mineral dust from field measurements in the Moroccan Sahara using electron microscopy, Atmos. Chem. Phys., 23, 3861–3885, https://doi.org/10.5194/acp-23-3861-2023, 2023.

Proestakis, E., Gkikas, A., Georgiou, T., Kampouri, A., Drakaki, E., Ryder, C. L., Marenco, F., Marinou, E., and Amiridis, V.: A near-global multiyear climate data record of the fine-mode and coarse-mode components of atmospheric pure dust, Atmos. Meas. Tech., 17, 3625–3667, https://doi.org/10.5194/amt-17-3625-2024, 2024.

Proestakis, E., Papachristopoulou, K., Georgiou, T., Chatoutsidou, S. E., Lazaridis, M., Gkikas, A., Fountoulakis, I., Tsikoudi, I., Petrakis, M. P., and Amiridis, V.: Atmospheric dust and air quality over large-cities and megacities of the world, Atmos. Chem. Phys., 25, 14777–14823, https://doi.org/10.5194/acp-25-14777-2025, 2025.

Pueschel, R. F., Russell, P. B., Allen, D. A., Ferry, G. V., Snetsinger, K. G., Livingston, J. M., & Verma, S. (1994). Physical and optical properties of the Pinatubo volcanic aerosol: Aircraft observations with impactors and a Sun-tracking photometer. Journal of Geophysical Research, 99(D6), 12,915–12,922. https://doi.org/10.1029/94JD00621

Randles, C. A., A. M. Da Silva, V. Buchard, P. R. Colarco , A. Darmenov.  R. Govindaraju, A. Smirnov, B. Holben, R. Ferrare, J. Hair, Y Shinozuka,  C J Flynn (2017). The MERRA-2 Aerosol Reanalysis, 1980 Onward. Part I: System Description and Data Assimilation Evaluation. *Journal of Climate*, 30(17), 6823-6850. https://doi.org/10.1175/JCLI-D-16-0609.1

Reid, E. A., J. S. Reid, M. M. Meier, M. R. Dunlap, S. S. Cliff, A. Broumas, K. Perry, and H. Maring (2003a), Characterization of African dust transported to Puerto Rico by individual particle and size segregated bulk analysis, *J. Geophys. Res.*, 108, 8591, doi:10.1029/2002JD002935, D19.

Reid, J. S., et al. (2003b), Comparison of size and morphological measurements of coarse mode dust particles from Africa, *J. Geophys. Res.*, 108, 8593, doi:10.1029/2002JD002485, D19.

Reid, J. S., Koppmann, R., Eck, T. F., and Eleuterio, D. P.: A review of biomass burning emissions part II: intensive physical properties of biomass burning particles, Atmos. Chem. Phys., 5, 799–825, https://doi.org/10.5194/acp-5-799-2005, 2005.

Reid, J. S., Brooks, B., Crahan, K. K., Hegg, D. A., Eck, T. F., O'Neill, N., et al. (2006). Reconciliation of coarse mode sea-salt aerosol particle size measurements and parameterizations at a subtropical ocean receptor site. Journal of Geophysical Research, 111(D2), D02202. https://doi.org/10.1029/2005JD006200

https://doi.org/10.5194/egusphere-2026-5531
Preprint. Discussion started: 18 September 2026





Reid, J. S., Reid, E. A., Walker, A., Piketh, S., Cliff, S., Al Mandoos, A., et al. (2008). Dynamics of southwest Asian dust particle size characteristics with implications for global dust research. Journal of Geophysical Research, 113, D14212. https://doi.org/10.1029/2007JD009752

Reid, J. S. et al. (2026), Delaminating the Marine Atmospheric Boundary and Saharan Air Layers: Observations and modeling by MAGPIE to understand marine boundary and lower free troposphere layer inhomogeneity over the Northwest Tropical Atlantic, Bull. Amer. Meteor. Soc., Online Publication: 14 Aug,2026, DOI: https://doi.org/10.1175/BAMS-D-25-0224.1

Rizzolo, J. A., Barbosa, C. G. G., Borillo, G. C., Godoi, A. F. L., Souza, R. A. F., Andreoli, R. V., Manzi, A. O., Sá, M. O., Alves, E. G., Pöhlker, C., Angelis, I. H., Ditas, F., Saturno, J., Moran-Zuloaga, D., Rizzo, L. V., Rosário, N. E., Pauliquevis, T., Santos, R. M. N., Yamamoto, C. I., Andreae, M. O., Artaxo, P., Taylor, P. E., and Godoi, R. H. M.: Soluble iron nutrients in Saharan dust over the central Amazon rainforest, Atmos. Chem. Phys., 17, 2673–2687, https://doi.org/10.5194/acp-17-2673-2017, 2017.

Rosenfeld, D., Woodley, W. L., Khain, A., Cotton, W. R., Carrió, G., Ginis, I., & Golden, J. H. (2012). Aerosol effects on microstructure and intensity of tropical cyclones. *Bulletin of the American Meteorological Society*, *93*(7), 987-1001. https://doi.org/10.1175/BAMS-D-11-00147.1

Ryder, C.L., Highwood, E.J., Lai, T.M., Sodemann, H. and Marsham, J.H., 2013. Impact of atmospheric transport on the evolution of microphysical and optical properties of Saharan dust. *Geophysical Research Letters*, *40*(10), pp.2433-2438. https://doi.org/10.1002/grl.50482

Ryder, C. L., McQuaid, J. B., Flamant, C., Rosenberg, P. D., Washington, R., Brindley, H. E., Highwood, E. J., Marsham, J. H., Parker, D. J., Todd, M. C., Banks, J. R., Brooke, J. K., Engelstaedter, S., Estelles, V., Formenti, P., Garcia-Carreras, L., Kocha, C., Marenco, F., Sodemann, H., Allen, C. J. T., Bourdon, A., Bart, M., Cavazos-Guerra, C., Chevaillier, S., Crosier, J., Darbyshire, E., Dean, A. R., Dorsey, J. R., Kent, J., O'Sullivan, D., Schepanski, K., Szpek, K., Trembath, J., and Woolley, A.: Advances in understanding mineral dust and boundary layer processes over the Sahara from Fennec aircraft observations, Atmos. Chem. Phys., 15, 8479–8520, https://doi.org/10.5194/acp-15-8479-2015, 2015.

Sayyah, A., Horenstein, M.N. and Mazumder, M.K., 2014. Energy yield loss caused by dust deposition on photovoltaic panels. *Solar Energy*, *107*, pp.576-604, doi:10.1016/j.solener.2014.05.030

Schafer, J. S., Eck, T. F., Holben, B. N., Thornhill, K. L., Anderson, B. E., Sinyuk, A., et al. (2014). Intercomparison of aerosol single scattering albedo derived from AERONET surface radiometers and LARGE in situ aircraft profiles during the 2011 DRAGON-MD and DISCOVER-AQ experiments. Journal of Geophysical Research: Atmospheres, 119, 7439–7452. https://doi.org/10.1002/2013JD021166

Schafer, J.S., Eck, T.F., Holben, B.N., Thornhill, K.L., Ziemba, L.D., Sawamura, P., Moore, R.H., Slutsker, I., Anderson, B.E., Sinyuk, A., Giles, D.M., Smirnov, A., Beyersdorf, A.J., Winstead, E.L., 2019. Intercomparison of aerosol volume size distributions derived from AERONET ground-based remote sensing and LARGE in situ aircraft profiles during the 2011-2014 DRAGON and DISCOVER-AQ experiments. Atmos. Meas. Technol. 12, 5289–5301. https://doi.org/10.5194/amt-12-5289-2019.

https://doi.org/10.5194/egusphere-2026-5531
Preprint. Discussion started: 18 September 2026




Schmid, B., Michalsky, J., Halthore, R., Beauharnois, M., Harrison, L., Livingston, J., et al. (1999). Comparison of aerosol optical depth from four solar radiometers during the fall 1997 ARM intensive observation period. Geophysical Research Letters, 26(17), 2725–2728. https://doi.org/10.1029/1999GL900513

Shaw, G.E., 1983. Sun photometry. *Bulletin of the American Meteorological Society*, *64*(1), pp.4-10. https://doi.org/10.1175/1520-0477(1983)064<0004:SP>2.0.CO;2

Shrestha, S., Holz, R. E., Marais, W. J., Buckholtz, Z., Razenkov, I., Eloranta, E., Reid, J. S., Elliott, H. E., Lata, N. N., Cheng, Z., China, S., Blades, E., Ortiz, A. D., Chewitt-Lucas, R., Allen, A., Blades, D., Agrawal, R., Reid, E. A., Ruiz-Plancarte, J., Bucholtz, A., Yamaguchi, R., Wang, Q., Eck, T., Lind, E., Pöhlker, M. L., Ault, A. P., and Gaston, C. J.: Transported African Dust in the Lower Marine Atmospheric Boundary Layer is Internally Mixed with Sea Salt Contributing to Increased Hygroscopicity and a Lower Lidar Depolarization Ratio, EGUsphere [preprint], https://doi.org/10.5194/egusphere-2025-4584, 2025.

Schuster, G. L., Vaughan, M., MacDonnell, D., Su, W., Winker, D., Dubovik, O., Lapyonok, T., and Trepte, C.: Comparison of CALIPSO aerosol optical depth retrievals to AERONET measurements, and a climatology for the lidar ratio of dust, Atmos. Chem. Phys., 12, 7431–7452, https://doi.org/10.5194/acp-12-7431-2012, 2012.

Sinyuk, A., Holben, B. N., Smirnov, A., Eck, T. F., Slutsker, I., Schafer, J. S., et al. (2012). Assessment of error in aerosol optical depth measured by AERONET due to aerosol forward scattering. Geophysical Research Letters, 39, L23806. https://doi.org/10.1029/2012GL053894

Sinyuk, A., Holben, B. N., Eck, T. F., Giles, D. M., Slutsker, I., Korkin, S., Schafer, J. S., Smirnov, A., Sorokin, M., and Lyapustin, A. , 2020: The AERONET Version 3 aerosol retrieval algorithm, associated uncertainties and comparisons to Version 2, Atmos. Meas. Tech., 13, 3375–3411, https://doi.org/10.5194/amt-13-3375-2020.

Sinyuk, A., Holben, B. N., Eck, T. F., Giles, D. M., Slutsker, I., Dubovik, O., Schafer, J. S., Smirnov, A., and Sorokin, M.: Employing relaxed smoothness constraints on imaginary part of refractive index in AERONET aerosol retrieval algorithm, Atmos. Meas. Tech., 15, 4135–4151, https://doi.org/10.5194/amt-15-4135-2022, 2022.

Smirnov, A., Holben, B. N., Dubovik, O., Frouin, R., Eck, T. F., & Slutsker, I. (2003). Maritime component in aerosol optical models derived from Aerosol Robotic Network data. Journal of Geophysical Research, 108(D1), 4033. https://doi.org/10.1029/2002JD002701

Sokolik, I., A. Andronova, T. C. Johnson, Complex refractive index of atmospheric dust aerosols, Atmospheric Environment. Part A. General Topics, Volume 27, Issue 16, 1993, Pages 2495-2502, ISSN 0960-1686, https://doi.org/10.1016/0960-1686(93)90021-P.

Sokolik, I. N., and O. B. Toon (1999), Incorporation of mineralogical composition into models of the radiative properties of mineral aerosol from UV to IR wavelengths, *J. Geophys. Res.*, 104(D8), 9423–9444, doi:10.1029/1998JD200048

Song, Q., Zhang, Z., Yu, H., Ginoux, P., and Shen, J.: Global dust optical depth climatology derived from CALIOP and MODIS aerosol retrievals on decadal timescales: regional and interannual variability, Atmos. Chem. Phys., 21, 13369–13395, https://doi.org/10.5194/acp-21-13369-2021, 2021.

https://doi.org/10.5194/egusphere-2026-5531
Preprint. Discussion started: 18 September 2026




Sun, D., Lau, K. M., & Kafatos, M. (2008). Contrasting the 2007 and 2005 hurricane seasons: Evidence of possible impacts of Saharan dry air and dust on tropical cyclone activity in the Atlantic basin. *Geophysical Research Letters*, *35*(15). https://doi.org/10.1029/2008GL034529

Swap, R., Garstang, M., Greco, S., Talbot, R. and Kållberg, P., 1992. Saharan dust in the Amazon Basin. *Tellus B*, *44*(2), pp.133-149. https://doi.org/10.3402/tellusb.v44i2.15434

Tanré, D., Kaufman, Y.J., Holben, B.E.A., Chatenet, B., Karnieli, A., Lavenu, F., Blarel, L., Dubovik, O., Remer, L.A. and Smirnov, A., 2001. Climatology of dust aerosol size distribution and optical properties derived from remotely sensed data in the solar spectrum. *Journal of Geophysical Research: Atmospheres*, *106*(D16), pp.18205-18217. https://doi.org/10.1029/2000JD900663

Todd, M.C., Washington, R., Martins, J.V., Dubovik, O., Lizcano, G., M'bainayel, S. and Engelstaedter, S., 2007. Mineral dust emission from the Bodélé Depression, northern Chad, during BoDEx 2005. *Journal of Geophysical Research: Atmospheres*, *112*(D6). https://doi.org/10.1029/2006JD007170

Toledano, C., Wiegner, M., Groß, S., Freudenthaler, V., Gasteiger, J., Müller, D., Müller, D., Schladitz, A., Weinzierl, B., Torres, B. and O'Neill, N.T., 2011. Optical properties of aerosol mixtures derived from sun-sky radiometry during SAMUM-2. *Tellus B: Chemical and Physical Meteorology*, *63*(4), pp.635-648. https://doi.org/10.1111/j.1600-0889.2011.00573.x

Toledano, C., González, R., Fuertes, D., Cuevas, E., Eck, T. F., Kazadzis, S., Kouremeti, N., Gröbner, J., Goloub, P., Blarel, L., Román, R., Barreto, Á., Berjón, A., Holben, B. N., and Cachorro, V. E.: Assessment of Sun photometer Langley calibration at the high-elevation sites Mauna Loa and Izaña, Atmos. Chem. Phys., 18, 14555–14567, https://doi.org/10.5194/acp-18-14555-2018, 2018.

Torres, B. and Fuertes, D.: Characterization of aerosol size properties from measurements of spectral optical depth: a global validation of the GRASP-AOD code using long-term AERONET data, Atmos. Meas. Tech., 14, 4471–4506, https://doi.org/10.5194/amt-14-4471-2021, 2021.

Wang, H., Liu, X., Wu, C., Lin, G., Dai, T., Goto, D., et al. (2024). Larger dust cooling effect estimated from regionally dependent refractive indices. Geophysical Research Letters, 51, e2023GL107647. https://doi.org/10.1029/2023GL107647

Washington, R., C. Bouet, G. Cautenet, E. Mackenzie, I. Ashpole, S. Engelstaedter, G. Lizcano, G.M. Henderson, K. Schepanski, & I. Tegen, Dust as a tipping element: The Bodélé Depression, Chad, Proc. Natl. Acad. Sci. U.S.A. 106 (49) 20564-20571, https://doi.org/10.1073/pnas.0711850106 (2009).

Westberry T. K., M. J. Behrenfeld, Y. R. Shi, H. Yu, L. A. Remer and H. Bian. 2023. "Atmospheric nourishment of global ocean ecosystems." Science 380 (6644): 515-519 [10.1126/science.abq5252]

Xian, P., Klotzbach, P. J., Dunion, J. P., Janiga, M. A., Reid, J. S., Colarco, P. R., and Kipling, Z.: Revisiting the relationship between Atlantic dust and tropical cyclone activity using aerosol optical depth reanalyses: 2003–2018, Atmos. Chem. Phys., 20, 15357–15378, https://doi.org/10.5194/acp-20-15357-2020, 2020.

https://doi.org/10.5194/egusphere-2026-5531
Preprint. Discussion started: 18 September 2026




Yang A., Q. Tan, C. Rajapakshe, M. Chin and H. Yu. 2022. "Global premature mortality by dust and pollution $PM_{2.5}$ estimated from aerosol reanalysis of the modern-era retrospective analysis for research and applications, version 2." Frontiers in Environmental Science 10 [10.3389/fenvs.2022.975755]

Yu, H., M. Chin, T. L. Yuan, H. Bian, L. A. Remer, J. M. Prospero, A. Omar, D. Winker, Y. Yang, Y. Zhang, Z. Zhang and C. Zhao. 2015. "The fertilizing role of African dust in the Amazon rainforest: A first multiyear assessment based on data from Cloud-Aerosol Lidar and Infrared Pathfinder Satellite Observations." Geophysical Research Letters 42 (6): 1984-1991 [10.1002/2015GL063040]

Yu, H., Tan, Q., Zhou, L., Zhou, Y., Bian, H., Chin, M., Ryder, C. L., Levy, R. C., Pradhan, Y., Shi, Y., Song, Q., Zhang, Z., Colarco, P. R., Kim, D., Remer, L. A., Yuan, T., Mayol-Bracero, O., and Holben, B. N.: Observation and modeling of the historic “Godzilla” African dust intrusion into the Caribbean Basin and the southern US in June 2020, Atmos. Chem. Phys., 21, 12359–12383, https://doi.org/10.5194/acp-21-12359-2021, 2021.

Yus-Díez, J., Escribano, J., Pandolfi, M., Alastuey, A., González-Flórez, C., Gonzalez-Romero, A., Gonçalves Ageitos, M., Ivančič, M., Klose, M., Kandler, K., Obiso, V., Panta, A., Reche, C., Rigler, M., Querol, X., and Perez Garćia-Pando, C.: Optical Properties and Shape-Dependent Complex Refractive Index Retrievals of Freshly Emitted Saharan Dust, EGUsphere [preprint], https://doi.org/10.5194/egusphere-2025-2571, 2025.

Zhang, Z., Li, J., Che, H., Dong, Y., Dubovik, O., Eck, T., Gupta, P., Holben, B., Kim, J., Lind, E., Saud, T., Tripathi, S. N., and Ying, T.: Long-term trends in aerosol properties derived from AERONET measurements, Atmos. Chem. Phys., 25, 4617–4637, https://doi.org/10.5194/acp-25-4617-2025, 2025.

Zhao, G., Zhao, C., Kuang, Y., Bian, Y., Tao, J., Shen, C., and Yu, Y.: Calculating the aerosol asymmetry factor based on measurements from the humidified nephelometer system, Atmos. Chem. Phys., 18, 9049–9060, https://doi.org/10.5194/acp-18-9049-2018, 2018.

Zhao, Y., Yue, X., Cao, Y., Zhu, J., Tian, C., Zhou, H., Chen, Y., Hu, Y., Fu, W., and Zhao, X.: Multi-model ensemble projection of the global dust cycle by the end of 21st century using the Coupled Model Intercomparison Project version 6 data, Atmos. Chem. Phys., 23, 7823–7838, https://doi.org/10.5194/acp-23-7823-2023, 2023.

Zheng, J., Zhang, Z., Yu, H., Garnier, A., Song, Q., Wang, C., Di Biagio, C., Kok, J. F., Derimian, Y., and Ryder, C.: Thermal infrared dust optical depth and coarse-mode effective diameter over oceans retrieved from collocated MODIS and CALIOP observations, Atmos. Chem. Phys., 23, 8271–8304, https://doi.org/10.5194/acp-23-8271-2023, 2023.

Zheng, J., Zhang, Z., DeSouza-Machado, S., Ryder, C.L., Garnier, A., Di Biagio, C., Yang, P., Welton, E.J., Yu, H., Barreto, A. and Gonzalez, M.Y., 2024. Assessment of dust size retrievals based on AERONET: A case study of radiative closure from visible-near-infrared to thermal infrared. *Geophysical Research Letters*, *51*(4), p.e2023GL1068, https://doi.org/10.1029/2023GL106808